Order Number 9405055

Circular magnetic x-ray dichroism in rare earth compounds

Lang, Jonathan Clark, Ph.D.

Iowa State University, 1993

U·M·I
300 N. Zeeb Rd.
Ann Arbor, MI 48106

Circular magnetic x-ray dichroism in rare earth compounds

by

Jonathan Clark Lang

A Dissertation Submitted to the
Graduate Faculty in Partial Fulfillment of the
Requirements for the Degree of
DOCTOR OF PHILOSOPHY

Department: Physics and Astronomy
Major: Condensed Matter Physics

Approved:

Signature was redacted for privacy.

In Charge of Major Work

Signature was redacted for privacy.

For the Major Department

Signature was redacted for privacy.

For the Graduate College

Iowa State University
Ames, Iowa

1993

TABLE OF CONTENTS

ACKNOWLEDGEMENTS

I am very thankful to the many people who assisted me in the course of my completing my degree here at Iowa State. Foremost, I would like to thank my wife, Jeannie, who put up with a four year diversion to getting on with life and provided the motivation to finish school, and my parents who encouraged and helped me though undergraduate and graduate school.

I would, also, like to thank all the people who influenced and guided my academic career. Leading the list, my advisor Dr. Alan Goldman, who taught me much more than physics, but also how to be a scientist. I am also deeply indebted to him for his many hours put in proofreading my papers and this thesis. I am also grateful to Dr. Bruce Harmon and Xindong Wang for their immense help in developing my understanding of circular dichroism, to Ken Finkelstein for his help in performing the experiments, and to Bill McCallum and Kevin Dennis for allowing me to use their laboratory facilities and for their assistance in taking many of my measurements.

In addition I would like to thank the many graduate students with whom I have made friends here at ISU. In particular, Stefan Kycia for our many discussion about x-ray physics, and Gora Mohanty and Kevin Jacobs for our many discussions about anything but physics.

This work was performed at Ames Laboratory under contract No. W-7405-ENG-82 with the Department of Energy. The United States government has assigned DOE report number IS-T-1686 to this thesis. The Cornell High Energy Synchrotron Source is supported by the National Science Foundation under grant No. DMR-87-19764.

GENERAL INTRODUCTION

An Explanation of the Dissertation Organization

This dissertation consists of three papers, one of which has been published, and two submitted, to scholarly journals. A general introduction including this format explanation and a literature review which sets up the problem precedes the three papers. Also preceding the papers is a more detailed explanation of the experimental methods used to measure circular magnetic x-ray dichroism. A general summary of the results appears after the three papers, followed by a list of the references cited in the general introduction, the general summary, and appendices. Three appendices appear at the end of the thesis; appendix A explains the origin of the dichroic signal; appendix B describes the polarization properties of synchrotron radiation; and appendix C describes the method used to determine the degree of circular polarization of the incident beam.

The experimental measurements, data analysis, and interpretation of the spectra has all been performed by the author of this work. During the course of this study he was assisted by many people, however, which are listed as co-authors on the included publications. The co-authors have contributed to this work in the following ways. Alan Goldman, my advisor, has assisted in the acquisition and analysis of the data. Xindong Wang, Bruce Harmon, and Vladimir Antropov performed the band structure calculations and assisted in the interpretation of the spectra. Ken Finkelstein and Stefan Kycia helped carry out the CMXD measurements at the Cornell synchrotron. Kevin Dennis, Bill McCallum, Dan

Branagan, Hong Wan, and George Hadjipanayis assisted in sample preparation and characterization.

Literature Review

The interaction of x-ray photons with matter has customarily been approximated by only considering the charge or Thompson scattering cross section. X-rays, however, are electromagnetic waves composed of electric and magnetic fields. Although the magnetic scattering cross section is reduced by a factor of 10^4 from the charge cross section, it should still be observable. Since the discovery of x-rays, there have been many experiments looking for magnetic effects in x-ray diffraction and absorption measurements but only recently have these effects been observed.

Magnetic x-ray diffraction was first demonstrated in 1972 by de Bergevin and Brunel for antiferromagnetic NiO.[1] The measurement of this effect was remarkable considering that the only x-ray sources available at the time were tube sources. Due to relatively small photon flux of these sources, one month of data collection was required to barely observe magnetic diffraction peaks. Only with the advent of synchrotron radiation sources in the late 70's did the time required for the observation of magnetic effects become reasonable (~1 day), and even then these measurements required considerable effort. The first study of magnetic x-ray scattering using these new sources was undertaken by Gibbs *et. al.*,[2] who measured the magnetic diffraction peaks of Ho metal. Interest in this technique was further stimulated by theoretical work which demonstrated that the polarization properties of magnetic peaks allowed for the separate determination of the orbital and spin

parts of the magnetic moment.[3] The small size of the magnetic signal, however, even at second generation synchrotron sources, has only made this separation possible on materials with large magnetic moments (i.e., Ho metal, μ (4f) = 10μ_b, L=6, S=2).[4] Some of the problems associated with the small size of the signal were overcome with the discovery of x-ray resonant exchange scattering (XRES).[4] In this technique a large enhancement of the magnetic peaks arising from virtual transitions to spin-polarized intermediate states encountered at resonance is observed as the incident x-ray energy is tuned through an absorption edge. This effect was first seen at the L_3 edge of Ho metal where a fifty-fold enhancement over non-resonant magnetic scattering was observed,[4] and more recently a factor of 1000 enhancement has been observed at the $M_{4,5}$ edges of uranium in UAs.[5] The large increase of the magnetic signal, however, is obtained at the expense of the well defined polarization properties which allowed for the separation of the moments in the non-resonant case. Thus, while XRES provides a method for the determination of magnetic structures using x-rays, it does not provide quantitative information about the size of the magnetic moments. Since it occurs at an absorption edge and involves transitions to intermediate states, XRES is the diffraction analog to the magnetic x-ray dichroism techniques described below.

The first unambiguous evidence of magnetic effects in x-ray spectroscopy measurements was seen in an experiment done by van der Laan *et. al.* in 1986.[6] They observed a change in the shape of the Tb $M_{4,5}$ edge spectra as the angle between the magnetization of a terbium iron garnet sample and the polarization direction of a linearly polarized x-ray beam was varied from 8° to 90°. In analogy with laser spectroscopy this effect has been coined "linear magnetic x-ray dichroism" (LMXD). This technique, however, has been restricted by the limited amount of

information which is provided by the spectrum and the small number of materials and edges at which it can be observed.

Soon afterward, however, Schütz *et. al.* [7] observed a difference in the absorption of left and right circularly polarized x-rays at the iron K edge for a magnetized iron sample. This difference in the absorption cross section for right and left circularly polarized light is called circular magnetic x-ray dichroism, (CMXD). Unlike linear dichroism, the interpretation of the CMXD signal is more straightforward and, to a crude first approximation, can be thought of as proportional to the difference in the spin density of unoccupied final states, (see appendix A). Experimental work progressed rapidly after these preliminary measurements with the same group observing an order of magnitude larger effect at the Gd and Tb $L_{2,3}$ edges a year later.[8] The technique was extended to the soft x-ray regime by Chen *et. al.* [9] soon afterward, where changes on the order of 10% in the L edge absorption of Ni metal were observed. Since that time, there have been experimental measurements on a variety of crystalline,[10-17] amorphous,[18] and multilayer[19-21] magnetic systems, along with an extensive amount of theoretical work[22-29] attempting to explain these spectra.

CMXD is defined as the difference, $\mu_C=\mu^+-\mu^-$, between the absorption coefficients of left and right circularly polarized x-ray beams in a magnetized sample, with $\mu^+(\mu^-)$ representing the absorption coefficient with the wave vector of the incoming x-ray photon parallel (antiparallel) to the magnetic moment. Since this absorption involves transitions from well understood core levels with well defined angular momenta, observed structure in the spectra can yield information about the spin polarization and spin-orbit coupling of final states.[22] Further, the information

obtained is element and orbital specific since the technique requires scanning through a specific absorption edge.

The $L_{2,3}$ edge CMXD spectra of transition metals,[23] including 5d impurities in 3d hosts,[24] have been well described using a simple spin polarized band structure model, and an atomic model has explained the spectra at the rare earth $M_{4,5}$ edges.[25] Such models, however, have failed to explain the sign, features, and magnitude of the CMXD spectra at the L_2 and L_3 edges of the rare earth elements, indicating the need for a more sophisticated interpretation of these spectra. CMXD measurements at these edges have shown two primary features, one above the absorption edge and another below the absorption edge. The feature above E_f (E_f is defined as the inflection point in the absorption edge spectra) has unambiguously been assigned to dipolar transitions involving the 5d unfilled states of the rare earth (RE) ion but the origin of the feature below the edge is still unknown. Carra and coworkers have suggested that this feature is due to quadrupole transitions to the 4f states,[26] pulled below the Fermi energy due to the presence of the core hole.[27] Their calculations predict that features in the CMXD spectra associated with quadrupolar and dipolar transitions should exhibit different angular dependencies, given by the expressions below,

$$\mu_c^{E1} = \frac{6\pi N}{k}(w_{11}-w_{1-1})\cos\theta, \tag{1}$$

$$\mu_c^{E2} = \frac{10\pi N}{k}\left[(w_{22}-w_{2-2})\sin^2\theta + (w_{21}-w_{2-1})\cos 2\theta\right]\cos\theta, \tag{2}$$

where $\mu_c = \mu_c^{E1} + \mu_c^{E2}$. Here N is the number of atoms per unit volume, k is the photon wave vector, the w_{lm} are the matrix elements of the transitions and θ is the

angle between the photon wave vector and the local magnetization direction. Thus, if one observes the dichroic signal at different values θ and normalizes by $\cos\theta$, features due to dipolar transitions should remain unchanged and features due to quadrupolar transitions should still exhibit additional angular dependence. Recent spin-polarized band structure calculations for all the heavy rare earth metals by Wang *et. al.*,[28] including the quadrupole contributions have reproduced the trends seen in the L_3 edge experiments of heavy rare earth compounds.[8,11] One of the purposes of this study, discussed in papers I and II, was an attempt to detect this angular dependence, and thus determine the multipole nature of the features in the L edge CMXD spectra of rare earth materials. It is important to understand the multipole nature of the transitions before quantitative information can be obtained from the CMXD signal.

While CMXD measurements can give orbital and element specific information, to become a useful tool for probing electronic and magnetic structures CMXD spectra should also be material specific. That is, sensitive to the changes in the band structure produced by different local environments. Recently, such sensitivity has been demonstrated in a variety of Ho compounds by Fischer *et. al.*.[12] Changes in coordination and nearest neighbor distances in various atomic environments should produce sufficient changes in the spin density of states to be detectable by CMXD measurements. A CMXD study can provide key information for understanding the properties of different magnetic materials, since CMXD spectra are proportional to the transition matrix elements and the local spin polarization of the final states. In the case of the L_2 and L_3 edges these final states correspond to empty levels within d bands, which in transition metals correspond to the magnetic 3d states. In rare earth compounds, these transitions are to the 5d band

primarily responsible for communicating the magnetic ordering among the rare earth 4f local moments. In addition, the CMXD spectra at the L_2 and L_3 edges differ from the ratio 1:-1 (see appendix A) by an amount dependent upon the spin-orbit coupling in the unoccupied d states. Thus, it is possible to separate the orbital and spin contributions to the local 3d (5d) magnetic moment for transition metals (rare earths).

Quantitative measurements of the degree of spin-orbit coupling are possible by employing recently derived sum rules, which relate the integrated intensity of the dichroic μ_c and normal μ_o absorption to the ground state values of the orbital $\langle L_z \rangle$ [29] and spin $\langle S_z \rangle$ [22] parts of the magnetic moment. It should also be noted that since the sum rules involve integrated quantities, the values of the moments obtained are ground state values. These are not affected by the creation of the core hole which can distort the shape and magnitude of the CMXD spectra, but not affect the integrated intensity values. At the rare earth $L_{2,3}$ edges, with initial p (l=1) states, final d (l=2) states, and 5d electron occupancy n≅1.8 (from the band theory), the sum rules reduce to the following simple expressions,

$$\int_{L_2+L_3} d\omega\, \mu_c \Big/ \int_{L_2+L_3} d\omega\, 3\mu_o = 16.4\, \langle L_z \rangle, \tag{3}$$

and,

$$\left\{ \int_{L_3} d\omega\, \mu_c - 2\int_{L_2} d\omega\, \mu_c \right\} \Big/ \int_{L_2+L_3} d\omega\, 3\mu_o = 12.3 \left(\langle S_z \rangle + \frac{7}{2} \langle T_z \rangle \right), \tag{4}$$

with $3\mu_o \approx \mu^+ + \mu^- + \mu^o$. In the expression above $\langle T_z \rangle$ is the spatial average of the magnetic dipole operator.[22] While this quantity can be neglected for the transition metal 3d band in $L_{2,3}$ edge CMXD measurements, and calculated analytically for rare earth 4f states in $M_{4,5}$ edge CMXD measurements, it is generally not possible to separate it from $\langle S_z \rangle$ in the expression above for rare earth $L_{2,3}$ edges. Thus, for the rare earth 5d states a quantitative value of only the orbital moment can be obtained. The value from equation 4 above could still be used for orbital specific, field and temperature dependent hysteresis measurements, however, since $\langle S_z \rangle$ and $\langle T_z \rangle$ remain coupled.

Recently the sum rules have been applied to CMXD measurements at the $L_{2,3}$ edges of cobalt to obtain the 3d moments[20] and to measurements at the $M_{4,5}$ edges of cerium compounds to obtain the 4f moments.[30] A portion of this study, discussed in paper III, sought to test the validity the above sum rules for the more extended 5d states by performing measurements at the Gd $L_{2,3}$ edges in amorphous and crystalline $GdFe_2$. The results are compared to a first principles theoretical calculation of the dichroic spectra for crystalline $GdFe_2$. Amorphous rare earth-transition metal materials are of considerable technological interest because of their many unique magnetic and magneto-optical properties.[31,32] For an understanding of these effects, knowledge of the spin-polarization and spin-orbit coupling of individual orbitals is necessary. CMXD analysis is, in principle, well suited to providing such information.

CMXD EXPERIMENTAL METHODS

CMXD measurements have been taken by three different experimental methods: conventional near edge spectroscopy, energy dispersive spectroscopy, and Faraday rotation measurements. The first two experimental setups were used in collecting the data for the following papers, while the experimental work using the third setup is unpublished at the present time. A detailed description of these setups is offered here in order to more clearly illustrate the data collection process and the advantages and disadvantages of each technique.

Conventional Near-edge Spectroscopy

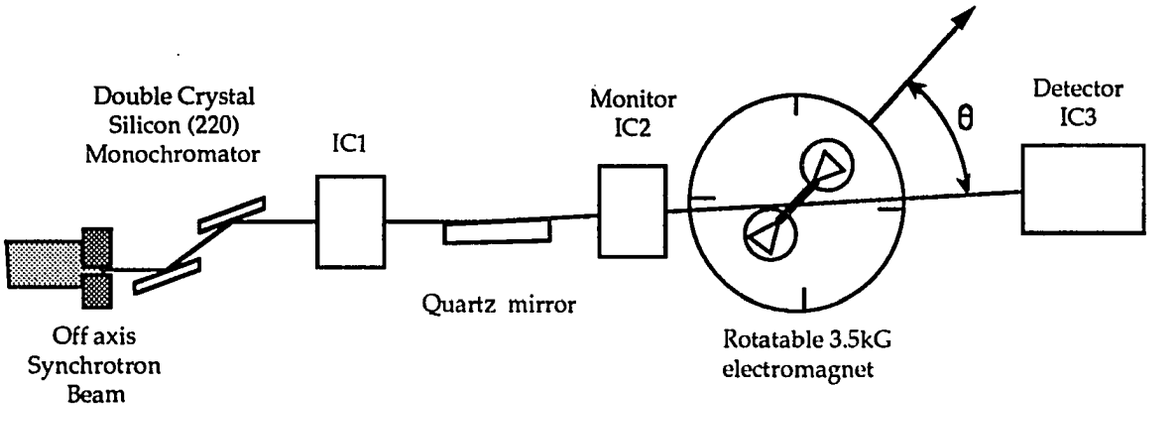

Figure 1 Schematic of the conventional double crystal monochromator setup used at CHESS B-2 and D beam lines.

The conventional near-edge spectroscopy setup used in papers I and III is illustrated in Figure 1. The apparatus consists of five parts: a double crystal monochromator diffracting in the vertical plane, a quartz mirror, a rotatable 3.5kG

electromagnet, a GaAs polarimeter, and three ionization chambers, two used as monitors and one as the detector. Circularly polarized x-rays were obtained by using the elliptical polarization of the synchrotron beam out of the electron orbital plane (see appendix B for a discussion of the polarization properties of synchrotron radiation). Upstream vertical slits of .25mm (13.8m from the source at B-2 line and 10.1 m from the source at D line) selected radiation which was .12-.14mrad out of the orbital plane, where the beam intensity dropped to ~10% of the peak intensity. The beam was then diffracted by a double crystal Si(220) monochromator yielding an energy resolution of ~1.5eV.

At a particular θ setting of the monochromator, Bragg's law,

$$\lambda = 2d\sin\theta, \tag{5}$$

will be satisfied not only for the primary wavelength but also for higher harmonics, (λ/n, n=2,3,4,...etc.). The harmonic content of the beam at a high-energy synchrotron storage ring can be appreciable since a large portion of the x-rays radiated lie in this portion of the spectrum. In absorption measurements, the presence of even a small amount of harmonic contamination can obscure the signal since the higher energy x-rays have a significantly lower absorption coefficient. Typically, in absorption measurements, the double crystal monochromator is detuned by about 50% to eliminate higher energy harmonics in the incident beam. That is, the second crystal is partially moved off the Bragg condition with respect to the first. For a double crystal monochromator the radiation transmitted through both crystals depends on the product of the two reflectivity curves. Since the rocking curve width of the higher energy harmonic is much smaller, (see Figure 2), detuning effectively

eliminates the higher energy x-rays as shown in Figure 3. In our case, however, detuning is undesirable since it also degrades the degree of circular polarization in the incident beam. Figure 4 shows that the rocking curve width of the π polarized radiation (E field in the scattering plane) is narrower than for the σ polarization (E field out of the scattering plane). When the monochromator is detuned (see Figure 5) more π polarized radiation will be rejected than σ radiation. Since the elliptically polarized light is composed of a greater amount of σ polarization (see Figure B.1 in appendix B) this larger reduction of the π component will increase the σ to π ratio and result in a lower degree of circular polarization. Therefore, in order to eliminate harmonic contamination of the incident beam, the x-rays were reflected from a flat quartz mirror placed after the monochromator rather than by detuning the monochromator itself. The mirror operates by total external reflection for grazing incidence x-rays. Thus at the proper angle (typically a few mrad) only the desired energy will be reflected and the higher energy harmonics will be absorbed.

The sample magnetization was reversed by placing it between the poles of a 3.5kG electromagnet. The plane of the sample was oriented as close as possible to the magnetic field direction in order to minimize demagnetization effects. Three ionization chambers were used, IC1 determined the off axis position ψ, IC2 served as the monitor, and IC3 was used as the detector. N_2 gas was used in the first two ionization chambers and Ar gas in the last.

The degree of circular polarization in the incident beam was measured to be $P_c=0.6\pm0.1$ at the Er L_3 edge. For linear polarization analysis, elastic scattering or Bragg reflections at a scattering angle of 90° can be used as a high-precision polarimeter over a wide energy range.[33] The determination of the degree of

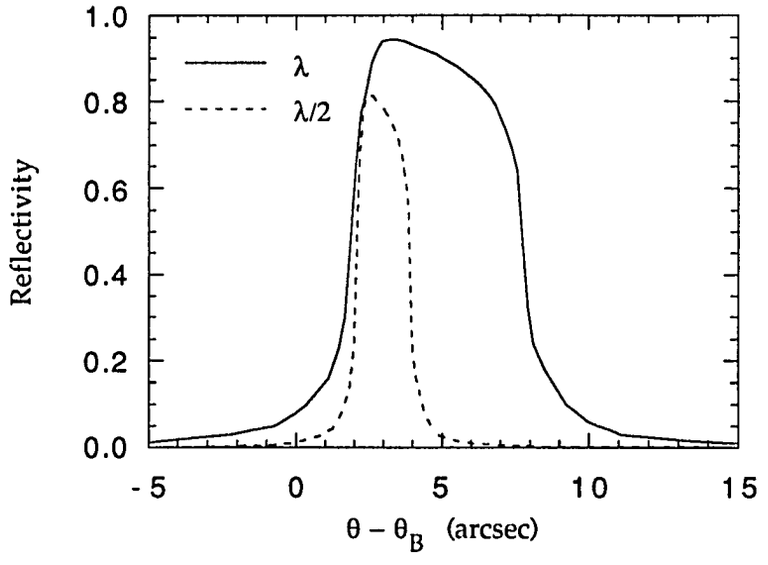

Figure 2 Reflectivity of an 8 keV and 16 keV x-ray for a Si (220) monochromator.

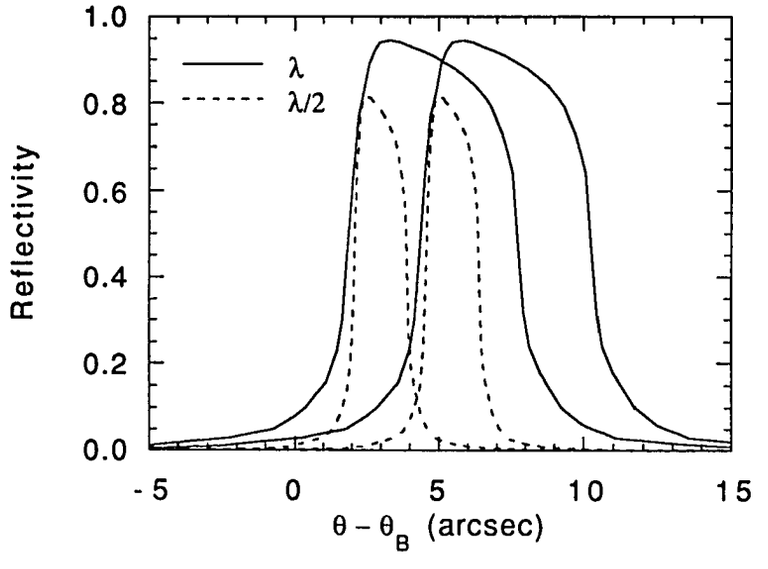

Figure 3 50% detuned monochromator showing negligible overlap of the higher energy x-rays.

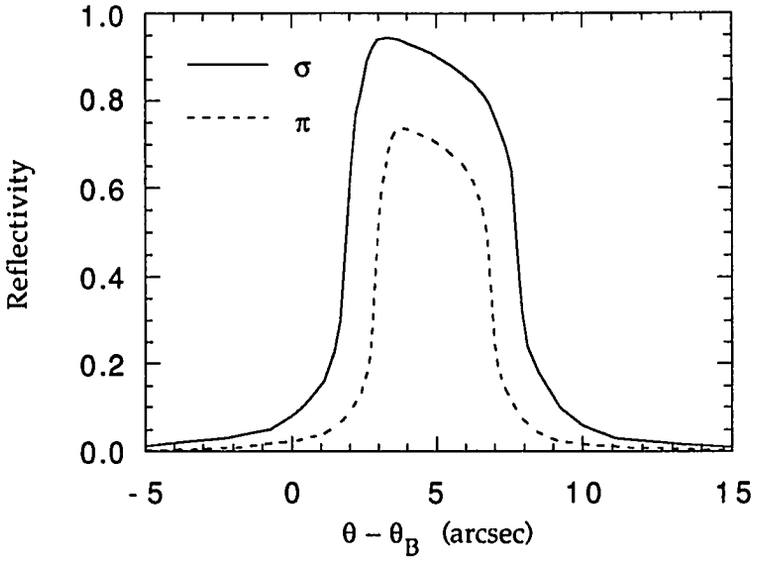

Figure 4 Reflectivity of σ and π polarized 8 keV x-rays for a Si (220) monochromator.

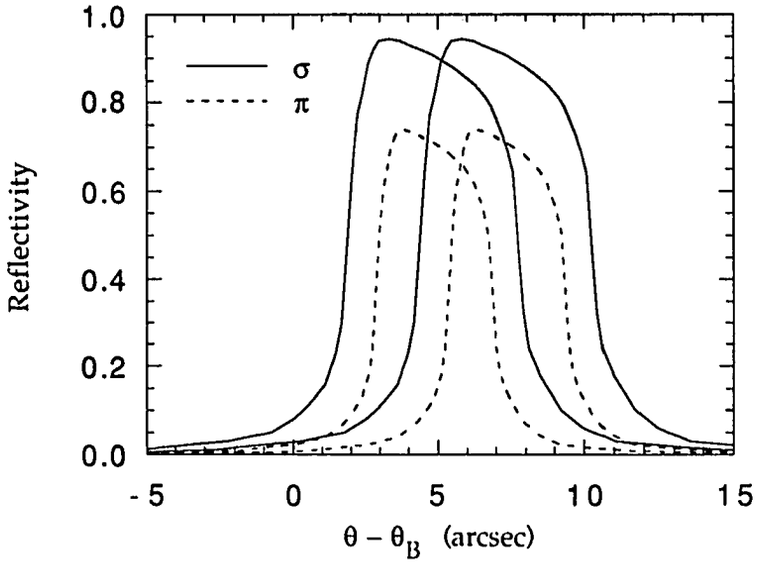

Figure 5 50% detuned monochromator showing the greater overlap of the σ polarized radiation.

circular polarization in the hard x-ray regime of interest for CMXD measurements on most magnetic materials (i.e. 5-10 keV) is more difficult however. The method employed for the determination of the degree of circular polarization in this experiment is based upon polarization-state mixing in multiple-beam diffraction processes from a single crystal of GaAs,[34] and is described in appendix C.

The polarization of the field was reversed every 2s at each step in an energy scan through the absorption edge thus producing two absorption spectra. I^+ is the transmitted intensity when the magnetic moment of the sample and the photon wave vector are in the same direction and I^- is the measured transmitted intensity when the two were in opposite directions. The absorption spectra (I^+,I^-) was related to the CMXD spectra μ_c by using,

$$\mu_c d = \frac{1}{M' P_c \cos\theta}\left(\ln\left(\frac{I_o^+}{I^+}\right) - \ln\left(\frac{I_o^-}{I^-}\right)\right), \qquad (6)$$

where $I_o^{\pm}$ are the incident intensities, measured by taking a spectra with the sample removed and only Kapton tape in the beam. In order to account for different experimental conditions and sample characteristics, the data were normalized by the factors found in the denominator of the right-hand side of equation 6. Small differences in the thicknesses and stoichiometry between samples were corrected for by normalizing the absorption edge data to the edge step of the absorption data for one the samples. Further normalization was done by dividing the data by the degree of polarization of the incident beam P_c and $\cos\theta$ where θ is the angle between the photon beam direction and the magnetic field direction. We also normalized to the fully saturated moment by dividing by M', the fraction of the sublattice saturation magnetization which the sample attained at room temperature in the field

used. The value of the thickness of the sample d can be obtained by matching the edge jump to known values for the material being studied. Generally this last step only needs to be done for comparison of the absolute magnitude of the CMXD spectra with theory, since the measurement of angular dependence only depends on the relative difference in the features above and below the edge and d factors out in the expressions for the sum rules.

Multiple scans were taken in order to increase statistical accuracy. Error bars on the data indicate the standard deviation as computed by taking each scan as an independent measurement and comparing with the mean. This is preferable to long integration times since the measurement involves the difference of two spectra and the beam characteristics of the synchrotron can change over the course of the electron bunch lifetime, (~1hr.). Using this setup, a typical CMXD spectra can be taken in approximately 1 day of data collection.

Energy Dispersive Spectroscopy

The experimental setup employing energy dispersive optics used for paper II is shown in Figure 6. The energy dispersive arrangement consists of five components: a total reflection mirror for harmonic rejection, a single bent crystal which diffracts in the horizontal plane and focuses the beam at the sample position, a N_2 ionization chamber used as a monitor, a 3.5kG electromagnet for reversing the magnetization direction of the specimen, and a linear pin diode detector array with small pixel size in the horizontal plane. Upstream vertical slits of .25mm (10.1m from the source) selected radiation which was .11mrad above the electron orbital plane, producing a degree of right circularly polarized light of $P_c \equiv 0.9$. This degree

of circular polarization is significantly higher than that obtained using the conventional setup, as explained below. The x-rays were reflected from a flat quartz mirror to eliminate harmonics. An elliptically bent (~1m radius) 22cm Si(111) monochromator with a 7.4° miscut selected an energy range of approximately 100eV. The asymmetric cut spread the beam out over the entire crystal increasing the energy band pass of the monochromator. The beam incident on the elliptically

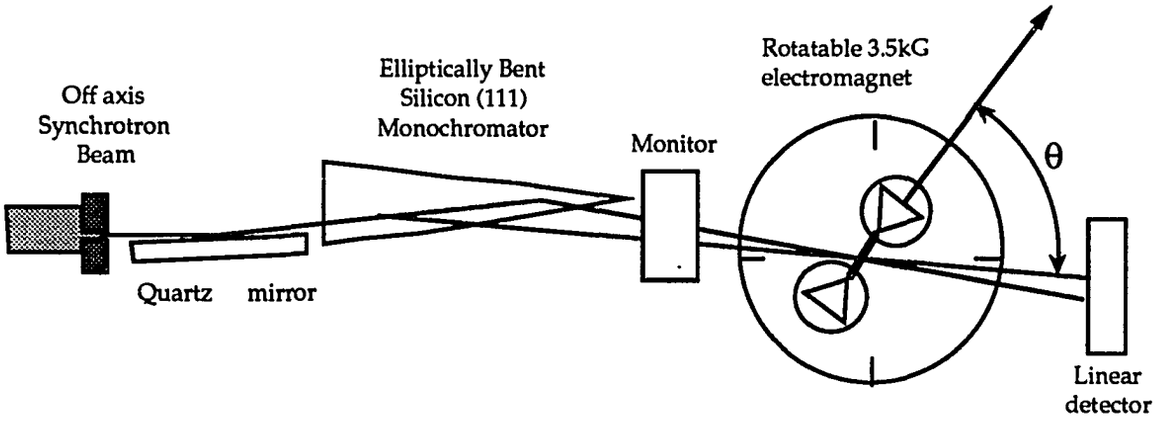

Figure 6 Schematic of the energy dispersive optics used at CHESS D line.

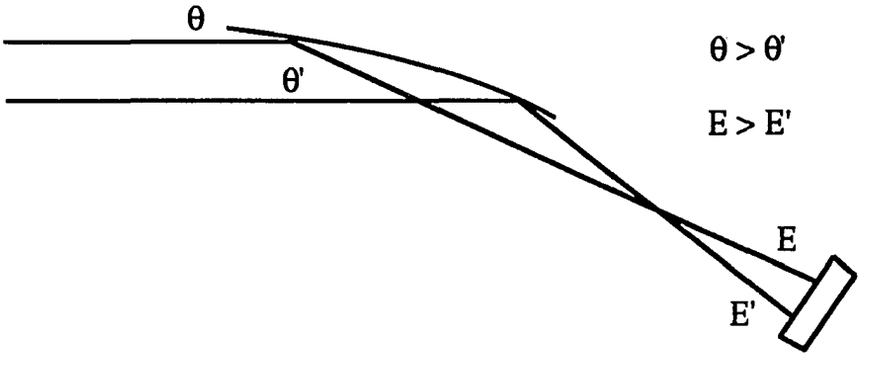

Figure 7 Top view of the elliptically bent crystal monochromator demonstrating the diffraction of two x-ray beams of different energies.

bent monochromator strikes with a range of angles θ, and therefore diffracts a range of energies which are focused at a point and diverge again (see Figure 7). With this setup, the spatial resolution of a linear detector positioned in the diverging beam directly behind the sample is effectively translates to energy resolution, since different portions of the monochromator will diffract different energies. Thus, the entire near-edge region can be observed without the need to scan the monochromator in a stepwise fashion. The sample was placed between the poles of a rotatable 3.5kG electromagnet located at the focus of the monochromator.

There are several advantages to the energy dispersive setup described above as opposed to the conventional experimental setup for near-edge absorption measurements. The greatest improvement for CMXD studies offered by this method is in the reduction of systematic errors because the energy dispersive spectrum samples the entire near-edge region in a single measurement. CMXD depends on the difference between two spectra taken with opposite magnetic field orientations on the sample. The fact that one avoids reversing the magnetic field at each energy step of the double crystal monochromator implies that the data is acquired much faster and is much less susceptible to systematic drifts in the apparatus.

Another advantage of this setup is the increased the degree of circular polarization P_c of the beam incident upon the sample offered by the horizontal diffraction plane employed in here. The σ polarization component of the synchrotron radiation is always greater than the π component, see Figure B.1 appendix B. As discussed in the description of the conventional spectroscopy setup, when the beam is diffracted in the vertical the reflectivity of the π polarization is lower than the σ (see Figure 4), further increasing the σ to π ratio. Since circular polarization is composed of a coherent sum of σ and π polarizations this reduces the

degree of circular polarization. Horizontal diffraction, on the other hand, effectively reverses the σ and π components of the beam, therefore making the σ to π ratio closer to 1 and increasing the degree of circular polarization. Furthermore, the time required to collect a CMXD spectra is reduced to ~3hrs. compared to ~1day for the conventional setup. Finally, the small focal size 1/2mm x 1/2mm reduces problems due to sample nonuniformity.

Using this apparatus, the polarization of the field was reversed every 60s and a spectrum taken. The absorption spectra (I^+ and I^-) were again related to the dichroic signal by equation 6. Drawbacks to this method arise in the data analysis, however. The monochromator will generally have different reflectivities for different portions of the bent crystal which results in structure in the incident beam. Normalizing by the monitor placed between the monochromator and the sample only compensates for the total flux in the beam, thus care must be taken to collect appropriate $I_0^{\pm}$ spectra to account for the structure in the incident beam. Also, linear pin diode detectors can produce a large dark current after exposure to the synchrotron beam. This can also contain structure as an image of the beam is burned onto pin diode array. Therefore spectra of the background must also be taken and subtracted from every measurement.

Faraday Rotation

An alternate way of measuring the CMXD signal is by measuring the rotation of plane of polarization for linearly polarized light.[33,35] Linear polarization can be expressed as a coherent sum of right and left circularly polarized light. Thus if it passes through a dichroic material the transmitted beam will have unequal amounts

of left and right polarization resulting in elliptically polarized light with it's major axis rotated by some angle. This measurement is different from the previous two since it measures the forward scattered component rather than the absorption, but can be related to a conventional CMXD measurement through a Kramers-Kroning transformation. While it is a more direct way of measuring the dichroism since it eliminates the need for subtracting two large numbers, the analysis of the data is more complicated because of the effects of optical activity not associated with magnetism.

The technique uses a highly linearly polarized incident beam which undergoes multiple bounces from a cannel cut Si(422) monochromator to obtain a σ to π ratio on the order of 10^6. This is illustrated in Figure 5 for just two reflections. After multiple reflections, the π component is effectively eliminated. The beam then passes through the sample and an analyzer oriented perpendicular to the monochromator measures the rotation of the polarization by scanning for the minimum intensity in the forward scattered beam.

PAPER I

CIRCULAR MAGNETIC X-RAY DICHROISM AT THE ERBIUM L_3 EDGE

Circular Magnetic X-ray Dichroism at the Erbium L_3 Edge

J.C. Lang, S.W. Kycia, X.D. Wang, B.N. Harmon and A.I. Goldman

Ames Lab - USDOE and Department of Physics and Astronomy,
Iowa State University, Ames, Iowa 50011

D.J. Branagan and R.W. McCallum

Ames Lab - USDOE and Department of Material Science and Engineering
Iowa State University, Ames, Iowa 50011

K.D. Finkelstein

Cornell High Energy Synchrotron Source and Department of Applied Engineering Physics
Cornell University, Ithaca, New York 14853

ABSTRACT

The spin dependent absorption of circularly polarized x-rays at the L_3 edge of Er has been studied in $Er_2Fe_{14}B$. Two distinct contributions, above and below the Fermi energy, are present. While they have been ascribed to dipolar and quadrupolar transitions to the empty 5d and 4f states respectively, we find that the angular dependence of both features was well described as dipolar. The results are compared to a theoretical spectrum for Er metal.

INTRODUCTION

The development of synchrotron radiation sources has stimulated the use of near edge absorption as a probe of the unoccupied electron states in solids. These sources have also allowed the study of magnetic properties of matter using x-rays.[1-4] One technique that has recently attracted great interest is spin dependent absorption of circularly polarized x-rays (or Circular Magnetic X-ray Dichroism = CMXD).[5] In CMXD the difference, $\mu_c=\mu^+-\mu^-$, between the absorption coefficients with the magnetic moment of the absorbing atom parallel (μ^+) and antiparallel (μ^-) to the wave vector of the incoming x-ray photon is determined. Since this absorption involves transitions from well understood core levels with well defined angular momenta, observed structure in the spectra can yield information about the spin polarization and spin-orbit coupling of final states. Further, the information obtained is element specific since the technique requires scanning through an absorption edge.

To become a useful tool for probing electronic and magnetic structures CMXD spectra should also be material specific. That is, the spectra for a particular magnetic ion should be sensitive to the surrounding structure so that details of that material's unique electronic and magnetic interactions can be ascertained. We are able to show, that in spite of a core hole broadening of about 4eV, the CMXD spectra measured for $Er_2Fe_{14}B$ is significantly different from that expected in pure metal. In addition we have measured the change in the CMXD spectra as a function of the angle between the moment of the absorbing atom and the photon wave vector in order to distinguish the multipole character of the transitions responsible for the observed structure in the spectra.

The rare earths are set apart from other magnetic materials by their unique

magnetic properties. Their highly localized partially filled 4f shells have negligible overlap with neighboring 4f shells and are responsible for large magnetic moments. Magnetic ordering in these materials arises from an exchange coupling between the 4f moments and the conduction electrons through which the conduction bands acquire a net magnetization.[6] This exchange is relatively well understood for elemental rare earth metals, but exchange and spin-orbit couplings complicate the analysis in rare earth transition metal compounds such as in the new hard magnetic materials (e.g. $(RE)_2Fe_{14}B$). In these materials the spin-orbit interaction is believed to play a major role in producing the large magnetic anisotropy. A CMXD study can provide key information for understanding the magnetic properties of such materials, since CMXD spectra are proportional to the transition matrix elements and the local spin polarization of the final states. In addition, the CMXD spectra at the L_2 and L_3 edges differ from the ratio 1:-1 by an amount dependent upon the spin-orbit coupling in the unoccupied d states.[7]

Recent experiments have demonstrated that in both the elemental rare earth[8] and $(RE)_2Co_{17}$ compounds,[9] the CMXD spectra across the L_3 edge of the rare earth consists of two contributions, one below the Fermi energy (E_f) and one above E_f, where E_f is defined as the inflection point in the L_3 edge absorption spectra. While the feature above E_f has unambiguously been assigned to dipolar transitions involving the 5d unfilled states of the RE ion, there has not been definitive confirmation of the nature of the peak below E_f. Motivated by resonance magnetic x-ray scattering experiments on Ho metal, which identified a feature below the edge as quadrupolar[10], Carra and Altarelli performed calculations predicting the angular behavior of the CMXD spectra assuming that the feature below the edge was due to quadrupolar 2p to 4f transitions.[12]

Quadrupolar transitions to the 4f states would occur for energies below E_f due to the greater 4f-core hole interactions.[11]

The dipole and quadrupole contributions to the absorption coefficient may be written as[12]

$$\mu_c^{E1} = \frac{6\pi N}{k}(w_{11}-w_{1-1})\cos\theta, \tag{1}$$

$$\mu_c^{E2} = \frac{10\pi N}{k}\left[(w_{22}-w_{2-2})\sin^2\theta + (w_{21}-w_{2-1})\cos 2\theta\right]\cos\theta, \tag{2}$$

with $\mu_c = \mu_c^{E1} + \mu_c^{E2}$. Here N is the number of atoms per unit volume, k is the photon wave vector, the w_{lm} are the matrix elements of the transitions and θ is the angle between the photon wave vector and the local magnetization direction. While the dipolar term exhibits only $\cos\theta$ dependence the quadrupolar contribution has a more complicated behavior due to the presence of the $\sin^2\theta$ and $\cos 2\theta$ terms. These distinct behaviors should be detectable in experiments which measure the spectra at different θ. Measurements by Fisher et al.[13] of the angular dependence of the dichroism below E_f at the Gd and Er L_3 edges in Gd_2Co_{17} and Er_2Co_{17} found no evidence for quadrupolar transitions to the 4f states. For Gd with a half filled 4f shell, however, the quadrupole transition matrix elements $(w_{22}-w_{2-2}) = 2(w_{21}-w_{2-1})$ in eq. (2), so that no angular dependence beyond $\cos\theta$ is expected.[11] For Er the measurement was done on the uniaxial Er_2Co_{17} compound so that the angular dependence of the quadrupole contribution is much reduced, as we describe below, after the appropriate powder averaging is performed.

EXPERIMENTAL DETAILS

The $Er_2Fe_{14}B$ sample was spun from a melt at 1300°C with a wheel speed of 10m/s in an argon atmosphere producing a polycrystalline ribbon. The ribbon was then micromilled producing a powder with particle sizes of ~1-10μm. This in turn was distributed uniformly on Kapton tape, with several layers of tape combined to produce a film of approximately 3 absorption thicknesses (~10mg/cm^2). As is true for other $RE_2Fe_{14}B$ compounds, $Er_2Fe_{14}B$ is tetragonal with the $P4_{2/mnm}$ space group.[14] The material is ferrimagnetic with the iron moment oriented antiparallel to the erbium moment. The Curie temperature is T_C=550K with the easy magnetization direction in the basal plane. The high quench rate achieved in the melt spinning process produces a nanocrystalline material in which the crystallites are randomly oriented. This nanocrystallinity allows for an easy reversal of the spin directions within the basal plane, thus producing a net magnetization of ~80% of the saturation value in fields of a few kilogauss. It must be kept in mind, however, that this is a net magnetization. Below the saturation field (~several Tesla) there is a distribution of spins whose average moment is oriented along the field direction. This is important since for quantitative measurements the angle between the moments and the photon wave vector direction must be known.

Either of two methods for measuring the CMXD spectra (μ_c) using circularly polarized x-rays may be employed. The sample magnetization can be reversed for a fixed polarization of the incoming radiation or the polarization can be reversed for a fixed magnetization. In this experiment we choose the former method. The measurements were taken at the Cornell High-Energy Synchrotron Source bending magnet B2 line making use of elliptical polarization

of the synchrotron beam out of the electron orbital plane. Upstream vertical slits of .35mm (13.8m from the source) selected radiation which was .10-.14mrad below the plane, where the beam intensity dropped to ~20% of the peak intensity. The beam was then diffracted by a double crystal Si(220) monochromater yielding an energy resolution of ~1eV. Typically in absorption measurements the double crystal monochromater is detuned by about 50% to eliminate higher energy harmonics in the incident beam. In our case, however, detuning is undesirable since it also degrades the degree of circular polarization in the incident beam. Therefore, in order to eliminate harmonic contamination of the incident beam, the x-rays were reflected from a flat quartz mirror placed after the monochromater. The sample was placed between the poles of a 3.5kG electromagnet and N_2 and Ar ionization chambers were used as the monitor and detector respectively. The degree of circular polarization in the incident beam was measured to be $P_c=0.6\pm0.1$ at the Er L_3 edge. The method used for the determination of the degree of circular polarization will be described elsewhere.[15] Here, we mention that it is based upon polarization-state mixing in multiple-beam diffraction processes from a single crystal of GaAs.[16]

The polarization of the field was flipped every 2s at each step in an energy scan through the Er L_3 edge thus producing two absorption spectra. I^+ is the transmitted intensity when the magnetic moment of the sample and the photon wave vector are in the same direction and I^- is the measured transmitted intensity when the two were in opposite directions. In order to relate the absorption spectra (I^+,I^-) to the CMXD spectra μ_c we used the same analysis as Schütz et al.[5] with two modifications. We have introduced a factor of 1/2 to match the definition of the dichroism in reference 11 and a factor of (-1) to account for the fact that the moment is primarily due to the 14 iron atoms in the

sample to which the erbium moment antiferromagnetically couples.

$$\frac{I^+ - I^-}{I^+ + I^-} = \tanh(P_c \mu_c d/2) \approx \frac{P_c}{2} \frac{\mu_c}{\mu} (\mu d)_{eff} \equiv \mu_c^* \qquad (3)$$

Here P_c ($0 \leq P_c \leq 1$ for left circularly polarized radiation below the orbit plane) is the degree of circular polarization of the incident beam and $(\mu d)_{eff}$ represents the effective absorption length of Er in the alloy. In the analysis of the angular dependence of the dichroism, P_c is constant and the spectra are normalized for minor differences in their effective thicknesses, thus we can set this expression equal to a quantity μ_c^* which incorporates all of the constants.

Multiple scans were taken in order to increase statistical accuracy. Error bars on the data indicate the standard deviation as computed by taking each scan as an independent measurement and comparing with the mean. Data were taken with the magnetic field at 30° and 60° with respect to the beam direction. For each angle, the sample thickness was chosen so that the beam was attenuated to the same extent and that the edge jump remained the same. The data were subsequently renormalized to the edge jump of one set of data. Further, the I^+ and I^- spectra were matched at points far from the edge in order to account for any preferred sensitivity of the ionization chambers with respect to the field direction of the electromagnet.

RESULTS AND DISCUSSION

The experimental μ_c^* at 30° and 60° were obtained from data taken in 0.5eV steps through the L_3 edge of Er. These data, divided by the respective cosines, are plotted in Fig. 1 along with theoretical curves calculated for pure hcp Er metal using the method discussed by Carra et al..[11] The theoretical method calculates the dipolar contributions using a self-consistent, spin polarized, relativistic LAPW band structure method, and uses an atomic model to evaluate the quadrupolar transitions to the highly localized 4f states. Actually, because of the great similarity of the band structures of all the heavy rare earth metals, the accurate dipolar part of the theoretical Gd CMXD spectra[11] was scaled to obtain the Er spectra. The scaling depends on the exchange interaction with the net 4f spin moment, and includes the changes of the spin up and spin down matrix elements determined by atomic calculations.[17]

It is important to realize that the calculations for the theoretical curves assumed full alignment of the moments along the magnetic field direction. This is not the case, however, in anisotropic materials such as $Er_2Fe_{14}B$, an easy plane ferromagnet, or Er_2Co_{17}, a uniaxial ferromagnet. Thus in equations (1) and (2) the average values of the angular terms, $\langle\cos\theta\rangle$, $\langle\sin^2\theta\cos\theta\rangle$, and $\langle\cos2\theta\cos\theta\rangle$, must be computed by integrating over a hemisphere about the magnetic field direction. To emphasize the importance of proper powder averaging, the inset of Fig. 1 shows the reduction of the difference in the angular dependence of the quadrupolar contributions (dashed lines) from that expected for full alignment of the moment (solid lines). In this integration a random orientation of crystalline directions was assumed, appropriate to the nanocrystallinity of the material.

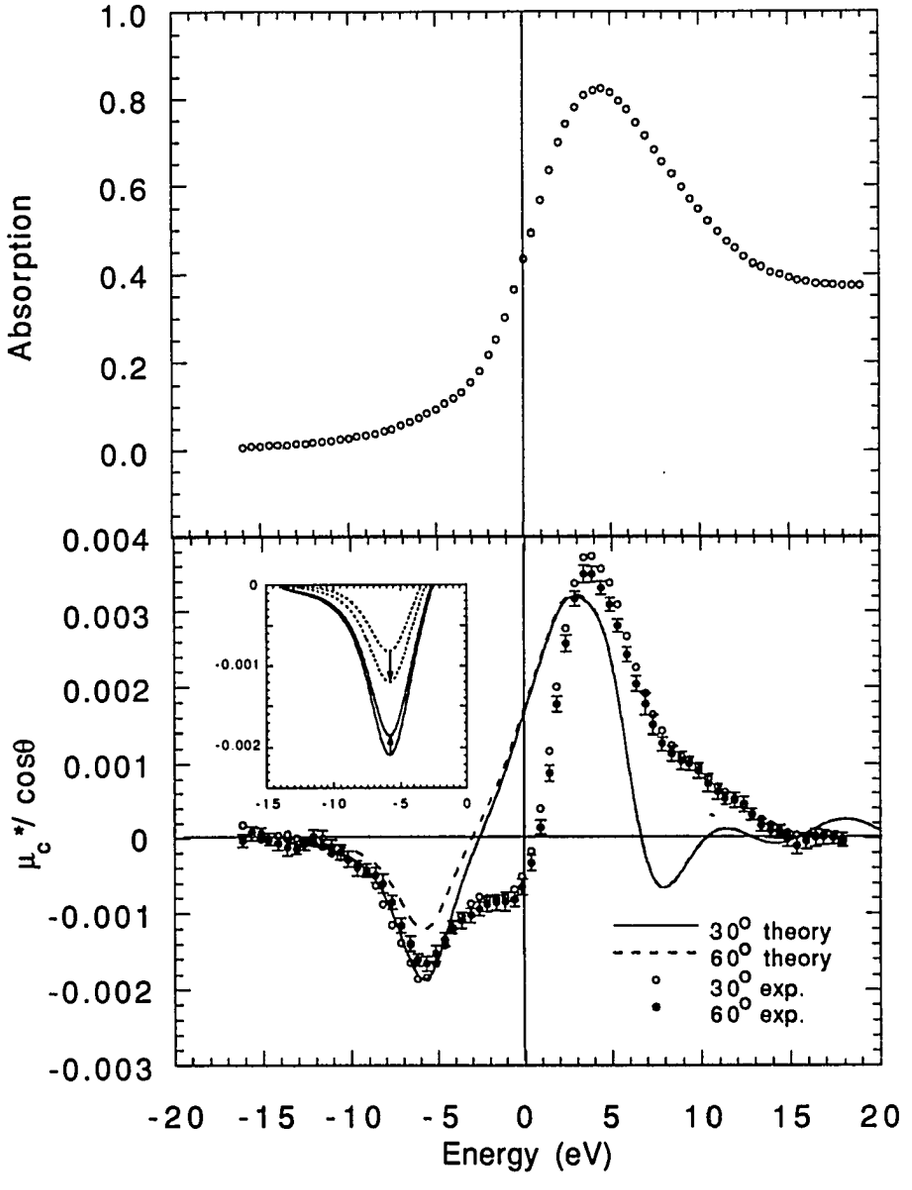

Figure 1 Top: Absorption discontinuity at Er L_3 edge. The background due to Fe and B has been subtracted. Bottom: CMXD spectra showing experimental data at 30° and 60° along with the theoretical curves for metallic Er as described in the text. Inset shows the affect of powder averaging on the theoretical CMXD spectra (solid line before averaging, dashed line after averaging).

After calculating the average angular values to obtain theoretical curves of μ_c, they were scaled so that the 30° quadrupole peak of the experimental data and the theoretical curves matched. This is equivalent to multiplying μ_c by the factors $P_c d$ in eq. (3) to give a theoretical μ_c^* curve.

The dichroic spectra in Fig. 1 are notable for two reasons. First, the dipolar part of the experimental spectrum is pushed to higher energy and has a different shape than the theoretical spectrum for pure Er metal. We note that the theoretical spectrum for pure Gd metal is in complete agreement with experiment,[11] and scaling the theoretical dipolar part of the spectra as described above also yields good agreement with the measured spectra for pure Tb metal. Secondly, there is no significant angular dependence in the experimental spectra for the features below the Fermi edge. The first observation shows there are easily measurable differences in the spectra for Er in different materials. In fact the difference between the theoretical curves for Er metal and the experimental curve for $Er_2Fe_{14}B$ can be qualitatively understood by reference to a recent calculation of the electronic structure of $Nd_2Fe_{14}B$.[18] This calculation showed that the Fe 3d states are dominant within about 2eV of the Fermi level and that the main part of the 5d density of states is pushed to higher energy. This also suggests the 5d contribution to the conduction electron moment is very small. The rather large positive dipolar contribution observed then arises from the spin up matrix elements being 20 to 30% larger than the corresponding spin down matrix elements. This is because the spin up 5d radial functions are more contracted and larger at the position of the 2p orbitals (see Fig. 8 of reference 6). While quantitative comparison between theory and experiment for $Er_2Fe_{14}B$ is desirable, with 68 atoms per cell, the precise calculations that would be required are formidable.

The predicted angular dependence of the feature below E_f for quadrupolar transitions is not observed, and only slight differences in the data at 30° and 60° are measured. These differences, however, occur equally in the peak above and below the edge and can be accounted for by an error in the measurement of the angle between the beam and field of ~2°. If to correct for this possible error, the peaks above the edge are matched to minimize the differences in the structure, no differences outside of error bars are seen between the two experimental curves. Therefore the feature below E_f exhibits the same angular dependence as the feature above E_f. This is indicative of dipolelike behavior which is not consistent with E2 transitions from $2p_{3/2}$ to 4f states.

The absence of the anticipated angular dependence for quadrupole transitions in our measurement for Er is unexpected in light of the reasonable match between the relative magnitudes of the peaks above and below E_f between theory and experiment, as well as the identification of a peak below E_f, in holmium, with quadrupolar transitions from x-ray scattering measurements.[10] A mechanism (such as hybridization or phonons) which would allow dipole matrix elements to couple the 2p states to states with strong 4f character could help explain the dipole angular dependence of the peak below E_f, but the E2 transitions would still be expected to contribute significantly. To resolve this issue, it would be desirable to have similarly accurate measurements on simple ferromagnetic single crystals, or more detailed calculations for these complicated compounds.

ACKNOWLEDGEMENTS

We would like to thank Dr. P. Carra for performing the atomic calculations of the Er quadrupolar contribution. Ames Laboratory is operated for the United States Department of Energy by Iowa State University under contract No. W-7405-ENG-82. Work at CHESS was supported by the National Science Foundation under grant No. DMR-87-19764.

REFERENCES

1 F. De Bergevin and M. Brunel, *Phys. Rev. Lett.* **58,** 737 (1972).

2 F. De Bergevin and M. Brunel, *Acta Cryst.* **A37,** 314 (1981).

3 G. van Der Laan, B.T. Thole, G.A. Sawatzky, J.B. Geodkoop, J.C. Fluggle, J.M. Esteva, R. Karnatak, J.P. Remeika and H.A. Dabkowska, *Phys. Rev. B* **34,** 6529 (1986).

4 D. Gibbs, D.E. Moncton, K.L. D'Amico, J. Bohr and B.H. Grier, *Phys. Rev. Lett.* **55,** 234 (1985).

5 G. Schütz, W. Wagner, W. Wilhelm, P. Kienle, R. Aeller, R. Frahm and G. Materlik, *Phys. Rev. Lett.* **58,** 737 (1987).

6 B.N. Harmon and A.J. Freeman, *Phys. Rev. B* **10,** 1979 (1974).

7 It is a simple exercise to show analytically that the L_2 and L_3 CMXD spectra are in this ratio if the empty conduction band states have only spin-polarization, but no spin-orbit coupling. It also provides a very useful test of our computer program since by turning off the spin-orbit coupling of the conduction electrons, we obtained the 1:-1 ratio to 3 significant digits.

8 G. Schütz, M. Knülle, R. Wienke, W. Wilhelm, W. Wagner, P. Kienle, and R. Frahm, *Z. Phys. B* **73,** 67 (1988).

9 P. Fischer, G. Schütz and G. Wiesinger, *Sol. Stat. Comm.* **76,** 777 (1990).

10 J.P. Hannon, G.T. Trammel, M. Blume and D. Gibbs, *Phys. Rev. Lett.* **61,** 1245 (1988).

11 P. Carra, B.N. Harmon, B.T. Thole, M. Altarelli, and G.A. Sawatzky, *Phys. Rev. Lett.* **66,** 2495 (1991).

12 P. Carra and M. Altarelli, *Phys. Rev. Lett.* **64,** 1286 (1990).

13 P. Fisher, G. Schütz, and S. Stähler, *J. Appl. Phys.* **69,** 6144 (1991).

14 J.F. Herbst, J.J. Croat, F.E. Pinkerton and W.B. Yelon, *Phys. Rev. B* **29**, 4179 (1984).

15 Qun Shen and K.D. Finkelstein, *Phys. Rev. B* **45**, 5075 (1992).

16 Q. Shen and K.D. Finkelstein, *Phys. Rev. Lett.* **65**, 3337 (1990).

17 The dipolar part of the CMXD spectra for all the heavy rare earth metals has been obtained in the same way and the separate quadrupolar parts evaluated within the atomic model. There is good qualitative agreement with the experimental results of reference 9. This work will be presented in another publication.

18 S.S. Jaswal, *Phys. Rev. B* **41**, 9697 (1991); and private communication.

PAPER II

ANGULAR DEPENDENCE OF CIRCULAR MAGNETIC X-RAY DICHROISM IN RARE EARTH COMPOUNDS

Angular Dependence of Circular Magnetic X-ray Dichroism in Rare Earth Compounds

J.C. Lang*, Xindong Wang, B.N. Harmon and A.I. Goldman

Ames Lab - USDOE and Department of Physics and Astronomy,
Iowa State University, Ames, Iowa 50011

K.W. Dennis, and R.W. McCallum

Ames Lab - USDOE and Department of Material Science and Engineering
Iowa State University, Ames, Iowa 50011

K.D. Finkelstein

Cornell High Energy Synchrotron Source and Department of Applied Engineering Physics
Cornell University, Ithaca, New York 14853

ABSTRACT

The angular dependence of the circular magnetic x-ray dichroism at the L_2 and L_3 edges of grain oriented $REFe_2$ compounds has been studied to ascertain the multipolar nature of the features above and below the absorption edge. Within experimental error, all features in the CMXD spectra are consistent with dipole transitions between 2p core levels and the unoccupied spin-polarized states. We discuss some possible reasons for the apparent absence of the predicted quadrupolar angular dependence of the features below E_f.

INTRODUCTION

Circular Magnetic X-ray Dichroism (CMXD) has increasingly been used as a probe of the magnetic properties of a variety rare earth materials.[1-3] An atomic model has provided a detailed description of the CMXD spectra at the rare earth $M_{4,5}$ edges,[4,5] but a complete explanation of the features and magnitude of the CMXD spectra at the $L_{2,3}$ edges of the rare earth elements has not yet been realized. The features above E_f (E_f defined as the inflection point in the absorption spectra) have unambiguously been assigned to dipolar transitions involving the unfilled 5d band of the RE ion. The origin of prominent peaks below the edge, however, is still uncertain. Carra and coworkers have suggested that these features are due to quadrupole transitions to the 4f states,[6] pulled below the Fermi energy due to the presence of the core hole.[7] Their calculations predict that features associated with quadrupolar and dipolar transitions should exhibit different angular dependencies given by the expressions,

$$\mu_c^{E1} = \frac{6\pi N}{k}(w_{11}-w_{1-1})\cos\theta, \tag{1}$$

$$\mu_c^{E2} = \frac{10\pi N}{k}\left[(w_{22}-w_{2-2})\sin^2\theta + (w_{21}-w_{2-1})\cos 2\theta\right]\cos\theta, \tag{2}$$

where $\mu_c = \mu_c^{E1} + \mu_c^{E2}$. Here N is the number of atoms per unit volume, k is the photon wave vector, the w_{lm} are the matrix elements of the transitions and θ is the angle between the photon wave vector and the local magnetization direction. Thus, if one observes the dichroic signal at different values θ and normalizes by

$\cos\theta$, features due to dipolar transitions should remain unchanged and features due to quadrupolar transitions should still exhibit additional angular dependence. As of yet, experiment has not confirmed the quadrupole nature of the feature below E_f,[2,8-10] but recent calculations for all the heavy rare earth metals by Wang *et. al.*[11] including the quadrupole contributions have reproduced the trends seen in the experimental spectra of reference 2. A similar experiment at the Fe K edge has also failed to demonstrate any quadrupole transitions between the core level 1s states and the 3d band.[12] All the measurements of the angular dependence performed thus far, however, have been on polycrystalline samples at room temperature in relatively modest magnetic fields. This has led to small values of M', the fraction of the T=0K rare earth sublattice magnetization attained for the field employed, due to structural anisotropy present in the samples and high values of the reduced temperature, T/T_c. It is important to realize that the expected quadrupole angular dependence is greatly reduced when the random orientation of the moments due to low M' values is considered. Therefore, high fields at low temperatures or high Curie temperatures are required for definitive measurements of the multipolarity of the transitions involved in the CMXD spectra. In this paper we achieve these higher values of M' by using grain aligned $REFe_2$ samples, which minimize effects due to anisotropy and temperature.

Recently, sum rules for the dichroic signal have been derived which make it possible to separately determine the orbital $\langle L_z \rangle$ [13] and spin $\langle S_z \rangle$ [14] contributions to the magnetic moment. Further, this information is orbital and element specific, due to the selectivity of the absorption edge. To date, no technique besides CMXD can easily provide such information. These rules have

already been applied to the $L_{2,3}$ edges of Co to obtain the 3d moments,[15] and at the Ce $M_{4,5}$ edges to obtain the 4f moments.[4] The derivation of these sum rules, however, assumes only dipole transitions play an important role in the dichroic spectra. Therefore, the determination of the multipole character of the peaks in these spectra is essential to extend these rules to the rare earth $L_{2,3}$ edges, involving transitions to the more extended 5d states. This is especially true for the heavy rare earth materials where the feature below the edge may be of comparable magnitude to features above the edge.

EXPERIMENTAL DETAILS

The samples were prepared by arc-melting 99.99% pure starting materials in a water cooled copper crucible under Argon atmosphere, and vacuum annealing for 3 days at 1100°C. $REFe_2$ compounds crystallize in the C15 cubic Laves phase with the RE and Fe moments oriented ferrimagnetically. The Curie temperatures for Dy-, Ho-, and $ErFe_2$ are 635, 605, and 593K respectively. The samples were micromilled and standard x-ray diffraction was used to check phase homogeneity. The powder was then diluted with an equal amount of boron, mixed with an epoxy, placed between two layers of Kapton, and allowed to cure in a 1.6T field oriented at 45° to the plane of the sample. This orientation allowed for the same thickness d (~3 absorption lengths below the L_3 edge) to be used for CMXD measurements at 30° and 60° with respect to the incident beam direction. Texture analysis confirmed that the samples were grain oriented along the easy axis of magnetization, ⟨100⟩ for $DyFe_2$ and $HoFe_2$, and along the ⟨111⟩ direction for $ErFe_2$. Magnetometer measurements at room temperature on unoriented and oriented samples indicated, that for equal applied fields, the bulk magnetization was increased by ~30% in the textured sample. The values of M' as determined by these magnetometer measurements and the temperature dependence of the rare earth sublattice magnetization as given by Clark[16], were found to be 0.63, 0.51, and 0.43 (±0.05) for the Dy-, Ho-, and $ErFe_2$ samples.

The CMXD measurements were performed at the Cornell High-Energy Synchrotron Source bending magnet D line using energy dispersive optics. Upstream vertical slits of .25mm(10.1m from the source) selected radiation

which was .11mrad above the electron orbital plane, producing a degree of right circularly polarized light of $P_c \cong 0.9$. The x-rays were then reflected from a flat quartz mirror to eliminate harmonics. An elliptically bent (~1m radius) Si(111) monochromator with a 7.4° miscut selected an energy range of approximately 100eV. The beam was then passed through a N_2 ionization chamber which was used as the monitor. The sample was placed between the poles of a rotatable 3.5kG electromagnet located at the focus of the monochromator. The spectra were collected using a linear detector supplied by Princeton Instruments Inc. placed ~1m from the magnet. There are several advantages to the energy dispersive setup described above as opposed to the conventional experimental set-up for near-edge absorption measurements. The horizontal diffraction plane employed increases the degree of circular polarization P_c of the beam incident upon the sample. The rate of data collection is also increased, allowing for better statistical accuracy of the experimental spectra. There is no need for scanning the monochromator in a stepwise fashion, thus eliminating a possible source of systematic error. The small focal size 1/2mm x 1/2mm reduces problems due to sample nonuniformity.

The polarization of the field was reversed every 60s and a spectrum taken. I^+ represents the transmitted intensity when the magnetic moment of the sample and the photon wave vector are in the same direction while I^- is the measured transmitted intensity when the two were in opposite directions. We relate these to the dichroic signal by

$$\mu_c d = \frac{1}{M' P_c \cos\theta}\left(\ln\left(\frac{I_o^+}{I^+}\right) - \ln\left(\frac{I_o^-}{I^-}\right)\right), \qquad (3)$$

where $I_o^{\pm}$ are the incident intensities. The data were normalized by dividing by P_C, M', and cosθ, where θ was the angle between the photon beam direction and the magnetic field direction.

RESULTS AND DISCUSSION

The experimental spectra at the L_2 and L_3 edges of $DyFe_2$, $HoFe_2$, and $ErFe_2$ taken with the field at 30° and 60° to the beam are shown in Figs. 1, 2, and 3. Within error all spectra show no differences in angular dependence in the features above and below the edge. Discrepancies between the two spectra below the Ho and Er L_3 edges are reproduced identically in the features above the edge. These departures from the expected cosine dependence arise from small differences in the effective sample thickness. The only substantial differences observed are found in the Ho L_2 edge. These differences are not believed to be a real effect, however, since the small signal was near our detection limit and the 30° data was plagued by stability problems during collection. Further measurements at this edge are planned to clarify this issue. Angular averaging calculations to account for spin fluctuations induced by temperature indicate that although the size of the angular dependence for pure quadrupole transitions should be diminished it should still be observable for the M' values of the grain aligned samples employed.

Fischer *et. al.* have suggested that the feature below the edge may arise from magnetic dipole transitions.[3] Magnetic dipole transitions, although satisfying angular momenta selection rules, give basically null contributions due to a null radial matrix element as pointed out by C. Brouder.[18] A more plausible explanation is that the feature is due to a small hybridization between the rare earth 4f and 5d states. While x-ray resonance exchange scattering (XRES) experiments performed on Ho metal[17] clearly show a quadrupole-like feature below the absorption edge, these measurements do not rule out the presence of

significant dipole transitions at this same energy. Furthermore, the calculations of the angular dependence used an isolated ion approximation, which completely neglected the possible hybridization of the 4f-shell with the conduction electron states both in the ground state and the excited states. When hybridization effects are taken into account the feature below the edge may have some mixed character due to the transitions from 2p core state to states with a mixture of d and f character. The mixing of these dipolar transitions below edge will reduce the relative weight of the quadrupolar transitions and make the experimental identification of the angular dependence of the feature more difficult. Although this hybridization must be very small because the 4f states remain highly localized, their effects may be enhanced by the dipolar matrix element which is two orders of magnitude larger than the quadrupolar matrix element.

In conclusion, the angular dependence of all the features in the dichroic spectra at the L_2 and L_3 edges of grain oriented $REFe_2$ was found to be consistent with dipolar transitions. One possible explanation for the lack of a clear quadrupolar signal is the presence of 4f-5d hybridization which may mask the effect in the dichroism spectra but not in XRES measurements. Even so, the feature below the edge should still exhibit some quadrupolar angular dependence in dichroism measurements. Future experiments on this question should be carried out at low temperatures and high fields in order to ensure that a maximum orientation of the moments (i.e., $M' \approx 1$) is achieved.

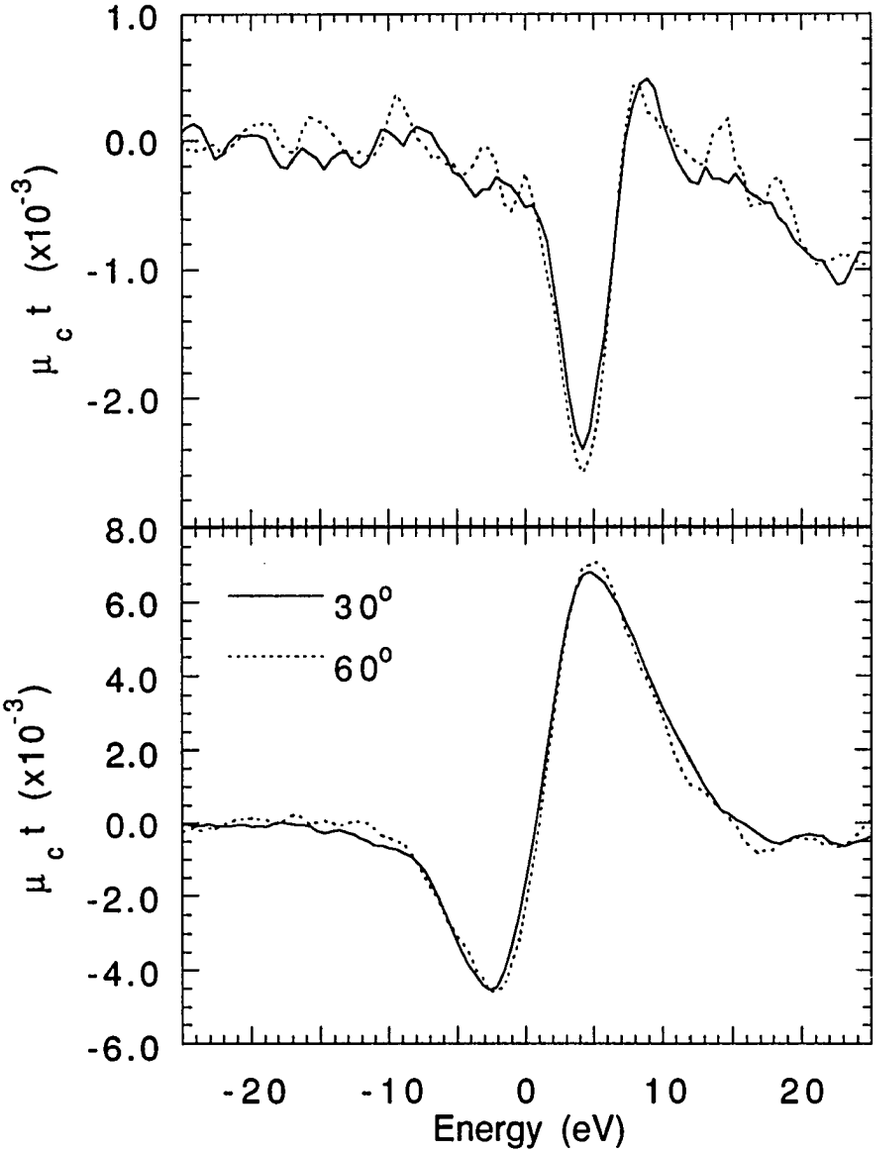

Figure 1 L_2 (Top) and L_3 (Bottom) dichroism in $DyFe_2$.

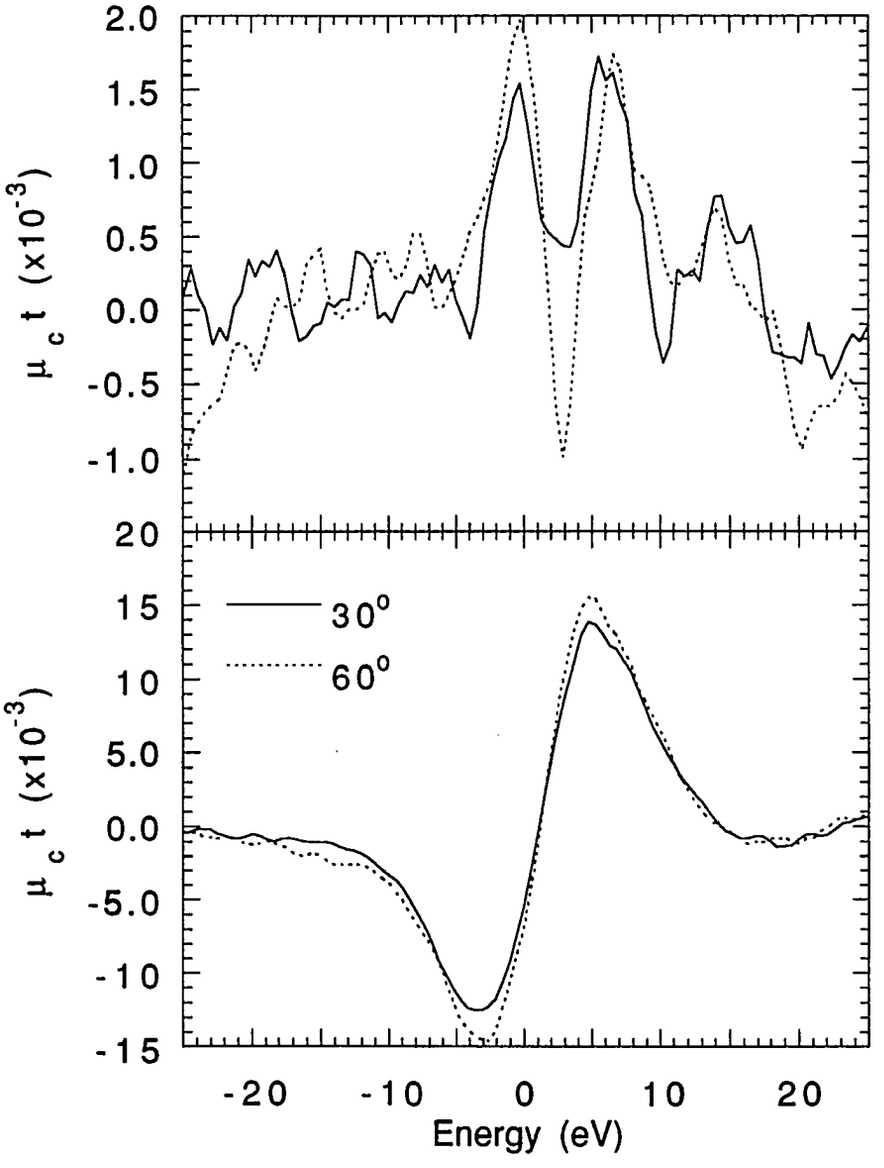

Figure 2 L_2 (Top) and L_3 (Bottom) dichroism in $HoFe_2$.

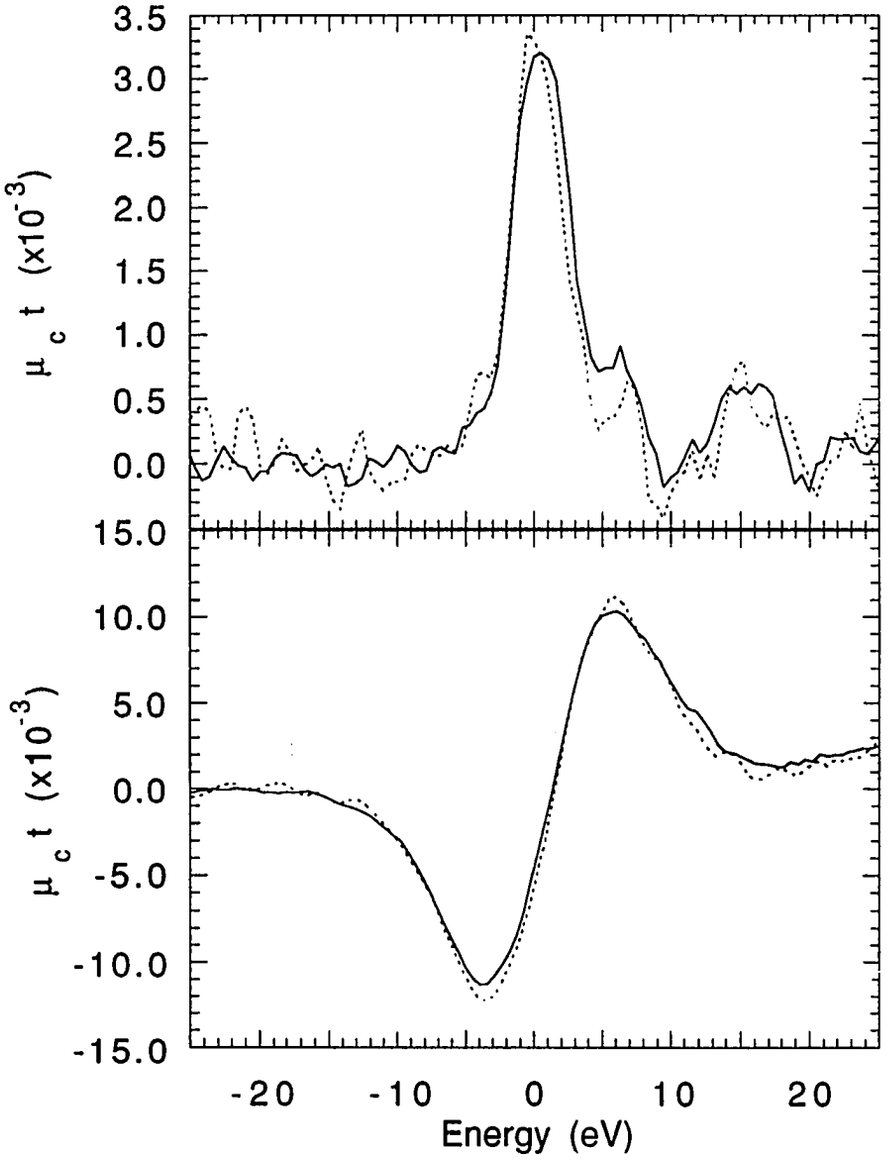

Figure 3 L_2 (Top) and L_3 (Bottom) dichroism in $ErFe_2$.

ACKNOWLEDGEMENTS

Ames Laboratory is operated for the United States Department of Energy by Iowa State University under contract No. W-7405-ENG-82. Work at CHESS was supported by the National Science Foundation under grant No. DMR-87-19764.

REFERENCES

* Present address, Advanced Photon Source, Bldg. 316, Argonne Natl. Lab., Argonne, IL 60439.

1 G. Schütz, M. Knülle, R. Wienke, W. Wilhelm, W. Wagner, P. Kienle, and R. Frahm, *Z. Phys. B* **73**, 67 (1988).

2 P. Fischer, G. Schütz, and G. Wiesinger, *Sol. State Comm.* **76**, 777 (1990).

3 P. Fischer, G. Schütz, S. Scherle, M. Knülle, S. Stähler, and G. Wiesinger, *Sol. State Comm.* **82**, 857 (1992).

3 F. Baudelet, E. Dartyge, A. Fontaine, C. Brouder, G. Krill, J.P. Kappler, and M. Piecuch, *Phys. Rev. B* **43**, 5857 (1991).

4 J.Ph. Schille, F. Bertran, M. Finazzi, C. Brouder, J.P. Kappler, and G. Krill, preprint submitted to *Phys. Rev. Lett.*.

5 J.Ph. Schille, Ph. Sainctavit, Ch. Cartier, D. Lefebvre, C. Brouder, J.P. Kappler, and G. Krill, *Sol. State Comm.* **85**, 787 (1993).

6 P. Carra and M. Altarelli, *Phys. Rev. Lett.* **64**, 1286 (1990).

7 P. Carra, B.N. Harmon, B.T. Thole, M. Altarelli, and G.A. Sawatzky, *Phys. Rev. Lett.* **66**, 2495 (1991).

8 P. Fisher, G. Schütz, S. Stähler and G. Wiesinger, *J. Appl. Phys.* **69**, 6144 (1991).

9 J.C. Lang, S.W. Kycia, X. Wang, B.N. Harmon, A.I. Goldman, D.J. Branagan, R.W. McCallum and K.D. Finkelstein, *Phys. Rev. B* **46**, 5298 (1992).

10 K. Shimomi, H. Maruyama, K. Kobayashi, A. Koizumi, H. Yamazaki, and T. Iwazumi, *Jpn. J. Appl. Phys.* **32-2**, 314 (1992).

11 X. Wang, T.C. Lueng, B.N. Harmon, and P. Carra, *Phys. Rev. B* **47**, 9087 (1993).

12 H. Yamazaki, H. Maruyama, K. Kobayashi, and K. Shimomi, *Jpn. J. Appl. Phys.* **32-2**, 317 (1992).

13 P. Carra, B.T. Thole, M. Altarelli, and X. Wang, *Phys. Rev. Lett.* **70**, 2307 (1993).

14 B.T. Thole, P. Carra, F. Sette, and G. van der Laan, *Phys. Rev. Lett.* **68**, 1943 (1992).

15 Y. Wu, J. Stöhr, B.D. Hermsmeir, M.G. Samant, and D. Weller, *Phys. Rev. Lett.* **69**, 2307 (1992).

16 A.E. Clark in Handbook on the Physics and Chemistry of Rare Earths Vol. 2 eds. K.A. Gschneidner Jr. and L. Eyrling (North-Holland, Amsterdam) Ch. 15.

17 J.P. Hannon, G.T. Trammel, M. Blume, and Doon Gibbs, *Phys. Rev. Lett.* **61**, 1245 (1988).

18 C. Brouder, *J. Phys. Cond. Matt.* **2**, 701 (1990).

PAPER III

CIRCULAR MAGNETIC X-RAY DICHROISM IN CRYSTALLINE AND AMORPHOUS $GDFE_2$

Circular Magnetic X-ray Dichroism in Crystalline and Amorphous $GdFe_2$

J.C. Lang*, Xindong Wang, V.P. Antropov, B.N. Harmon and A.I. Goldman

Ames Lab - USDOE and Department of Physics and Astronomy, Iowa State University, Ames, Iowa 50011

H. Wan, G. C. Hadjipanayis

Department of Physics University of Delaware, Newark, Delaware 19716

K.D. Finkelstein

Cornell High Energy Synchrotron Source and Department of Applied Engineering Physics Cornell University, Ithaca, New York 14853

ABSTRACT

The spin dependent absorption of circularly polarized x-rays at the K edge of Fe and the L_2 and L_3 edges Gd in amorphous and crystalline $GdFe_2$ has been studied. Large differences in the magnitude of the dichroic signal are observed between the two samples. The application of recently derived sum rules indicates substantial quenching of the orbital moment in the amorphous sample. The results are compared to a theoretical spectrum for crystalline $GdFe_2$.

INTRODUCTION

With the availability of present and next generation synchrotron radiation sources, Circular Magnetic X-ray Dichroism (CMXD) has increasingly been used as a probe of the bulk magnetic properties of a variety of crystalline[1-5] and multilayer systems.[6,7] CMXD is defined as the difference, $\mu_C=\mu^+-\mu^-$, between the absorption of left and right circularly polarized x-ray beams by a magnetized sample, with $\mu^+(\mu^-)$ representing the absorption coefficient for x-rays with the wave vector parallel (antiparallel) to the ferromagnetically ordered magnetic moment. Since x-ray absorption involves transitions from well understood core levels with well defined angular momenta, observed structure in the dichroic spectra can yield information about the ground state spin polarization and spin-orbit coupling of final states.[8] Further, the information obtained is element and orbital specific since the technique requires scanning through a specific absorption edge.

To become a useful tool for probing electronic and magnetic structures CMXD spectra should also be material specific, i.e., sensitive to the changes in the band structure produced by different local environments. Recently, such sensitivity has been demonstrated in a variety of Ho compounds by Fischer *et. al.*.[9] In this paper, we compare the CMXD spectra of amorphous $GdFe_2$ with its crystalline counterpart and a first principles theoretical calculation of the dichroic spectra for crystalline $GdFe_2$. First principles calculations of the dichroic spectra are made possible due to the relatively simple cubic structure of $GdFe_2$. Changes in coordination and nearest neighbor distances in glassy $GdFe_2$ should produce sufficient changes in the electronic structure to be detectable by CMXD

measurements. Furthermore, amorphous rare earth-transition metal materials are of considerable interest because of their many unique magnetic and magneto-optical properties.[10,11] For an understanding of these effects, knowledge of the spin-polarization and spin-orbit coupling of individual orbitals is necessary. CMXD analysis is, in principle, well suited to providing such information.

The L edge CMXD spectra of transitions metals,[12] including 5d impurities in 3d hosts,[13] have been well described using a simple spin polarized band structure model. Such a model, however, fails to explain the sign, features, and magnitude of the CMXD spectra at the L_2 and L_3 edges of the rare earth elements, indicating the need for a more sophisticated interpretation of these spectra. The first measurements of the CMXD spectra performed at the L edges of Gd and Tb metal demonstrated two prominent features, one below and one above the absorption edge. The feature above E_f (E_f is taken as the inflection point in the absorption edge spectra) has been unambiguously assigned to dipolar transitions involving the 5d unfilled states of the RE ion, but the origin of the feature below the edge is still uncertain. Carra and coworkers have suggested that this feature is due to quadrupole transitions to the 4f states, pulled below the Fermi energy due to the strong Coulomb interaction between the core hole and these states.[14] As of yet, experiments have not confirmed the quadrupole nature of the feature below E_f,[9,15,16] but recent calculations for all the heavy rare earth metals by Wang *et. al.* [17] which include quadrupole contributions have reproduced the trends seen in the experimental spectra of reference 2.

The rare earths are set apart from other magnetic materials by their unique magnetic properties. Their highly localized partially filled 4f shells have negligible overlap with neighboring 4f shells and are responsible for large

magnetic moments. Magnetic ordering in these materials arises from an exchange coupling between the 4f moments and the conduction electrons through which the conduction bands acquire a net magnetization.[18] This exchange is relatively well understood for elemental rare earth metals, but intermetallic bonding and spin-orbit coupling complicate the analysis in rare earth transition metal compounds. A CMXD study can provide key information for understanding the magnetic properties of such materials since CMXD spectra are proportional to the transition matrix elements and the local spin polarization of the final states. In the case of the L_2 and L_3 edges these final states correspond to empty levels within 5d bands which are primarily responsible for transmitting the ordering among the 4f local moments. In addition, the CMXD spectra at the L_2 and L_3 edges differ from the ratio 1:-1 by an amount dependent upon the spin-orbit coupling in the unoccupied d states.

Quantitative measurements of the degree of coupling are possible by employing recently derived sum rules, which relate the integrated intensity of the dichroic μ_c and normal μ_o absorption to the ground state values of the orbital $\langle L_z \rangle$ [19] and spin $\langle S_z \rangle$ [8] parts of the magnetic moment. Until now, a separate determination of the spin and orbital magnetic moments has been possible only by non-resonant magnetic x-ray scattering.[20] Owing to the small size of the magnetic cross section, however, this technique has been limited to samples with large magnetic moments (i.e., Ho μ (4f) = $10\mu_b$, L=6, S=2).[21] Further, this technique is not orbital specific and requires measurement of several magnetic diffraction peaks with different q values. CMXD, on the other hand, can give the values of moments on the order of $0.01\mu_b$ with measurements at just the L_2 and L_3 absorption edges. It should also be noted that since the sum rules involve

integrated quantities, the values of the moments obtained are ground state values not affected by the creation of the core hole which can distort the shape and magnitude of the CMXD spectra.

EXPERIMENTAL DETAILS

The crystalline $GdFe_2$ sample was prepared by arc-melting 99.99% pure starting materials in a water cooled copper crucible under argon atmosphere, then vacuum annealed for 3 days at 1100°C. The sample was then micromilled and standard x-ray diffraction was used to check phase homogeneity. This in turn was distributed uniformly on Kapton tape, with several layers of tape combined to produce a film of approximately 2.0 absorption thicknesses below the Gd L_3 edge. The amorphous sample was prepared by sputtering the materials onto a Kapton substrate under vacuum and overlaying the film with a thin (<200Å) Si layer. The film thickness was found to be ~1.5μm with 4 films used for the absorption measurements, (~1.4 absorption thicknesses just below the Gd L_3 edge). The stoichiometry of the material was checked using EDS and found to be Gd_xFe_{1-x} (x=.315 +/- .020) and standard x-ray diffraction measurements confirmed the glassy nature of the sample.

The CMXD measurements were taken at the Cornell High-Energy Synchrotron Source bending magnet D line making use of elliptical polarization of the synchrotron beam out of the electron orbital plane. Upstream vertical slits of .25mm(10.1m from the source) selected radiation which was .11mrad above the electron orbital plane, producing a degree of right circularly polarized light of $P_c \cong 0.66 \pm 0.10$. The beam was diffracted by a double crystal Si(220) monochromator yielding an energy resolution of ~1.5eV in the vicinity of the Fe K and Gd L edges where the measurements were performed. In order to eliminate harmonic contamination of the incident beam, the x-rays were reflected from a flat quartz mirror placed after the monochromator. The

magnetization of the sample was reversed by a 3.5kG electromagnet, with the magnetic field oriented at 30° with respect to the beam direction.

The polarization of the field was flipped every 2s at each step in an energy scan through the edges thus producing two absorption spectra. I^+ is the transmitted intensity when the magnetic moment of the sample and the photon wave vector are in the same direction and I^- is the measured transmitted intensity when the two were in opposite directions. We relate these to the dichroic signal by,

$$\mu_c d = \frac{1}{M' P_c \cos\theta}\left(\ln\left(\frac{I_o^+}{I^+}\right) - \ln\left(\frac{I_o^-}{I^-}\right)\right), \qquad (1)$$

where $I_o^{\pm}$ are the incident intensities. In order to account for different experimental conditions and sample characteristics, the data were normalized by the factors found in the denominator of the right-hand side of eq. 1. Small differences in the thicknesses and stoichiometry were corrected for by normalizing the absorption edge data from the glassy sample to the edge step of the absorption data for the crystalline sample. Further normalization was done by dividing the data by the degree of polarization of the incident beam P_C and $\cos\theta$ where θ was the angle between the photon beam direction and the magnetic field direction.

Both crystalline and amorphous $GdFe_2$ order ferrimagnetically with the iron moment oriented antiparallel to the gadolinium moment. The Curie temperatures are T_C=785K for the crystalline and T_C=500K[11] for the amorphous sample, yielding reduced temperature values of T/T_c=.38 and T/T_c=.6. Therefore, the data must also corrected for a reduced M', the fraction of the T=0K

saturation magnetization attained at room temperature for the field employed. Magnetometer measurements performed by us, combined with ferromagnetic resonance measurements by Vittoria *et. al.*[22] place the values of the iron and gadolinium sublattice magnetizations at room temperature for a 3.5kG field at .66±.08 and .85±.06 $M(Fe, T=0K)_{sat}$, and .67±.09 and .66±.08 $M(Gd, T=0K)_{sat}$ for the crystalline and amorphous samples respectively. The effective thickness of the sample d was determined by matching the experimental edge step with known absorption values for crystalline $GdFe_2$.[23]

RESULTS AND DISCUSSION

The experimental spectra μ_c taken in 0.5eV steps at the Gd L_2 and L_3 edges and the Fe K edge, along with theoretical curves for crystalline $GdFe_2$ are shown in Figs. 1, 2 and 3. A summary of the data is presented in table 1 which displays the integrated intensity and the width of the CMXD signal at each edge, as well as the value of the 5d orbital moment determined by using the sum rule derived in reference 19.

The relativistic band structure calculation was carried out within the local spin density approximation (LSDA) suitable for describing the ground state properties of heavy rare earths. Dipolar contributions to the dichroic spectra were calculated using an atomic-sphere-approximation tight binding linear-muffin-tin-orbital (ASA-TB-LMTO) band structure code with the combined correction,[24] and using an atomic model to evaluate quadrupole contributions arising from transitions to the 4f states at the Gd L_2 and L_3 edges. The theoretical spectra have been convoluted with a 3.5 eV Lorentzian to account for the finite core hole lifetime. The spectra were also convoluted with a 1.5 eV (FWHM) Gaussian to account for the experimental resolution, and with an energy dependent broadening to account for the conduction state lifetime.[25] The calculations assume full alignment of the moments. Thus, as stated earlier, we have normalized the experimental data to the T=0K saturation magnetization for direct comparison of theory and experiment.

Only small differences are observed between the amorphous and crystalline spectra at the Fe K edge. Discrepancies between the data sets can be seen 2eV below the edge (feature A in fig. 1) and 16eV above the edge (just below

feature D). The overall magnitude of the dichroism for both samples is approximately equal as indicated by the integrated intensity of features B and C in table I. The similarity of the shape and magnitude of the signals suggest that the Fe moment of the amorphous sample is not substantially different from the crystalline sample, although the size of the CMXD signal at the K edge has been shown not to scale with the 3d or 4p moments in Fe compounds.[26] The band structure calculations attribute features A, B, and C to hybridization between the 4p and 3d states in the iron. Thus, the difference in feature A between the amorphous and crystalline spectra presumably arises from differences in the details of the 4p-3d hybridization. The theoretical spectrum, while giving a very reasonable match to the shape of experimental crystalline spectrum, overestimates the magnitude of the signal by a factor of three to four. The theoretical calculations, however, also overestimate the magnitude of the overall absorption by a factor of 1.5, which could account for some of the observed discrepancy.

The sign and magnitude of the dichroism signal at the rare earth L_2 and L_3 edges has been a mater of controversy. Before a discussion of the results at the Gd L edges, then, a brief explanation of the origin of the dichroic signal in these materials is useful. To lowest approximation, the CMXD spectra can be expressed as,

$$\mu_c \propto M(\uparrow)\rho(\uparrow) - M(\downarrow)\rho(\downarrow) \qquad (2)$$

where $M(\uparrow(\downarrow))$ is the matrix element of the transition from the 2p core level to the spin up (down) state and $\rho(\uparrow(\downarrow))$ is the density states for majority (minority)

spins. In rare earth compounds the inclusion of distinct matrix elements is essential since the M(↑) matrix elements to the majority spin states are 20-30% larger than the M(↓) matrix elements. This arises from the fact that the 4f-5d exchange radially splits the spin bands with the result that the 5d spin up radial functions are larger in magnitude and more contracted at the position of the 2p orbitals (see Fig. 8 of Ref. 17). The magnitude of this exchange scales with the spin of the 4f states, and is therefore strongest for Gd compounds. A positive net 5d moment implies that there are more unoccupied spin down states above E_f $\{\rho(\downarrow) > \rho(\uparrow)\}$ and therefore one naively expects a net positive (negative) CMXD spectra at the L_2 (L_3) edge. Just the opposite is observed, however, due to the larger M(↑) matrix elements, which make $M(\uparrow)\rho(\uparrow) > M(\downarrow)\rho(\downarrow)$ reversing the sign of the CMXD signal. It should be noted that the expected 1:-1 ratio of the CMXD signal at the L_2 and L_3 edges for systems without conduction electron spin-orbit coupling is not affected since the $2P_{1/2}$ and $2P_{3/2}$ matrix elements differ by less than 10%. Therefore, the difference from the 1:-1 ratio for the CMXD signal at these edges still provides information about the degree of 5d conduction electron spin-orbit coupling and the sum rule derived for $\langle L_z \rangle$, as discussed below, still holds.

The difference in the matrix elements is also partly responsible for the observed enhancement of the dichroic signal in the amorphous sample. The Fe coordination around each Gd atom has been determined to be 6.5±0.6 in amorphous $GdFe_2$ as compared to 12 for the crystalline compound while the nearest neighbor distances remain roughly the same.[27] This smaller coordination number reduces the 5d-3d exchange thus diminishing the spin polarization of the 5d band. This interpretation is supported by recent

calculations performed by Brooks *et. al.*[28] on a series of $REFe_2$ compounds, where the 3d-5d hybridization results in greater 3d spin down, (parallel of RE moment), charge transfer to the rare earth 5d band, and thus a larger 5d spin-polarization. Smaller amounts of hybridization reduce both the 5d and 3d moments, but since they are oppositely oriented their sum remains essentially constant. Therefore, while the difference in the spin density of the 5d band $\{\rho(\uparrow) - \rho(\downarrow)\}$ is smaller in the amorphous sample, the larger $M(\uparrow)$ matrix elements combined with the greater number of unoccupied spin up states above the Fermi energy produces the observed enhanced signal. In this case then, a *smaller* net 5d spin moment corresponds to a *larger* CMXD signal.

The sum rules for the CMXD spectra are not affected by the above discussion since they are independent of the matrix elements. At the rare earth $L_{2,3}$ edges, with initial p (l=1) states, final d (l=2) states, and 5d electron occupancy $n \cong 1.8$ (from the band theory), the sum rules reduce to the following simple expressions,

$$\int_{L_2+L_3} d\omega\, \mu_c \Big/ \int_{L_2+L_3} d\omega\, 3\mu_o = 16.4\, \langle L_z \rangle, \tag{3}$$

and,

$$\left(\int_{L_3} d\omega\, \mu_c - 2\int_{L_2} d\omega\, \mu_c \right) \Big/ \int_{L_2+L_3} d\omega\, 3\mu_o = 12.3 \left(\langle S_z \rangle + \frac{7}{2} \langle T_z \rangle \right), \tag{4}$$

with $3\mu_o \approx \mu^+ + \mu^- + \mu^o$. In the expression above $\langle T_z \rangle$ is the spatial average of the magnetic dipole operator.[8] While this quantity can be neglected for the

transition metal 3d band in $L_{2,3}$ edge CMXD measurements, and calculated analytically for rare earth 4f states in $M_{4,5}$ edge CMXD measurements, it is generally not possible to separate it from $\langle S_z \rangle$ in the expression above for rare earth $L_{2,3}$ edges. Thus, for the rare earth 5d states a quantitative value of only the orbital moment can be obtained. The value from eq. 4 above could still be used for orbital specific, field and temperature dependent hysteresis measurements since $\langle S_z \rangle$ and $\langle T_z \rangle$ remain coupled.

The integrated values of the dichroic spectra were obtained by summing the signal over the entire observed energy range at each edge, while the integrated values of μ_o were determined by modeling the background with a 4 eV broadened arctangent function centered 8.5 eV above the edge. The orbital moment values of 0.018±.005 and 0.005±.003 were obtained for the crystalline and amorphous samples respectively. The error in the size of the moments arises primarily from the error in the degree of circular polarization. Since both the amorphous and crystalline data are scaled by this value, the error in relative difference between the amorphous and crystalline samples is ~15% smaller. The smaller value of the 5d band spin polarization in the amorphous sample is also responsible, in part, for the substantially smaller $\langle L_z \rangle$ as compared to the crystalline sample, since a smaller net 5d moment implies a smaller orbital moment. We believe, however, that the dominant mechanism responsible for the quenching of the orbital moment is the more random crystal field symmetry present in the amorphous sample. The average crystal field at a particular Gd site should be substantially more asymmetric in the amorphous compound as compared to the crystalline sample leading to decreased effectiveness of the spin-orbit coupling in producing an orbital polarization of the 5d conduction bands.

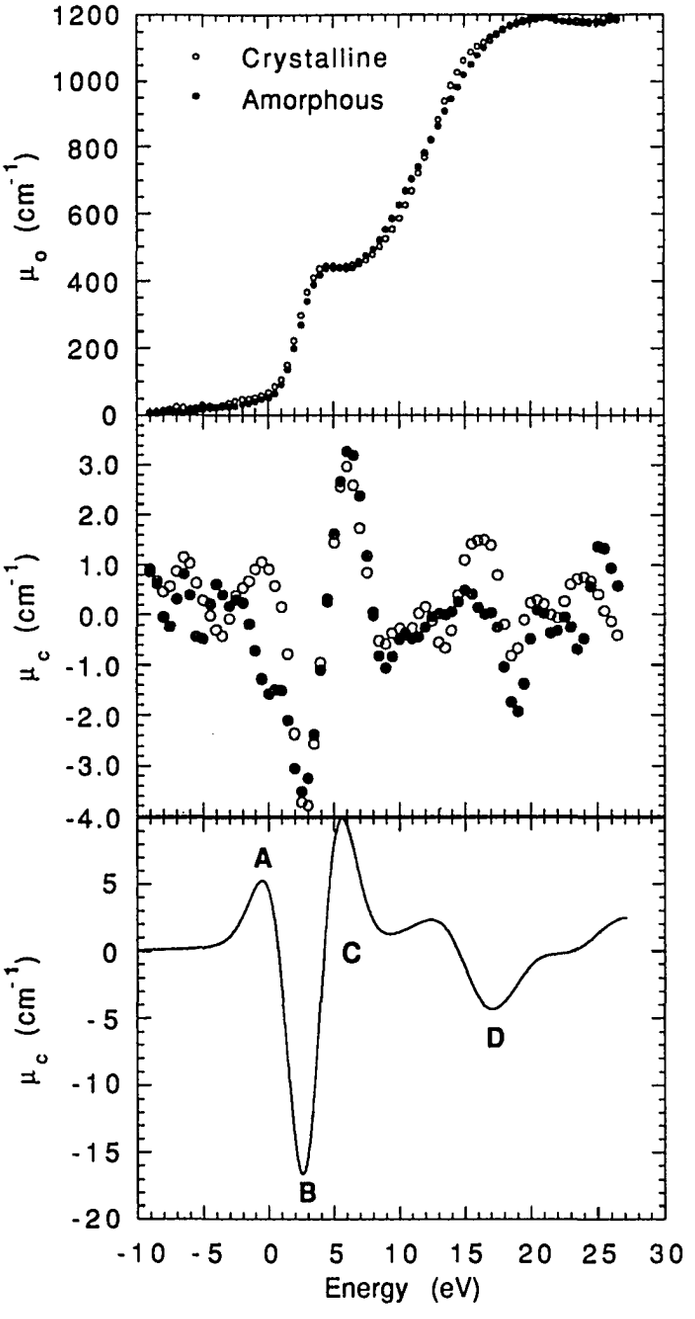

Figure 1 Dichroism at the Fe K edge. Top: Absorption of crystalline and amorphous samples. Middle: Dichroism signal μ_c of crystalline and amorphous samples. Size of dots indicates approximate error bars. Bottom: Theoretical curve for crystalline $GdFe_2$.

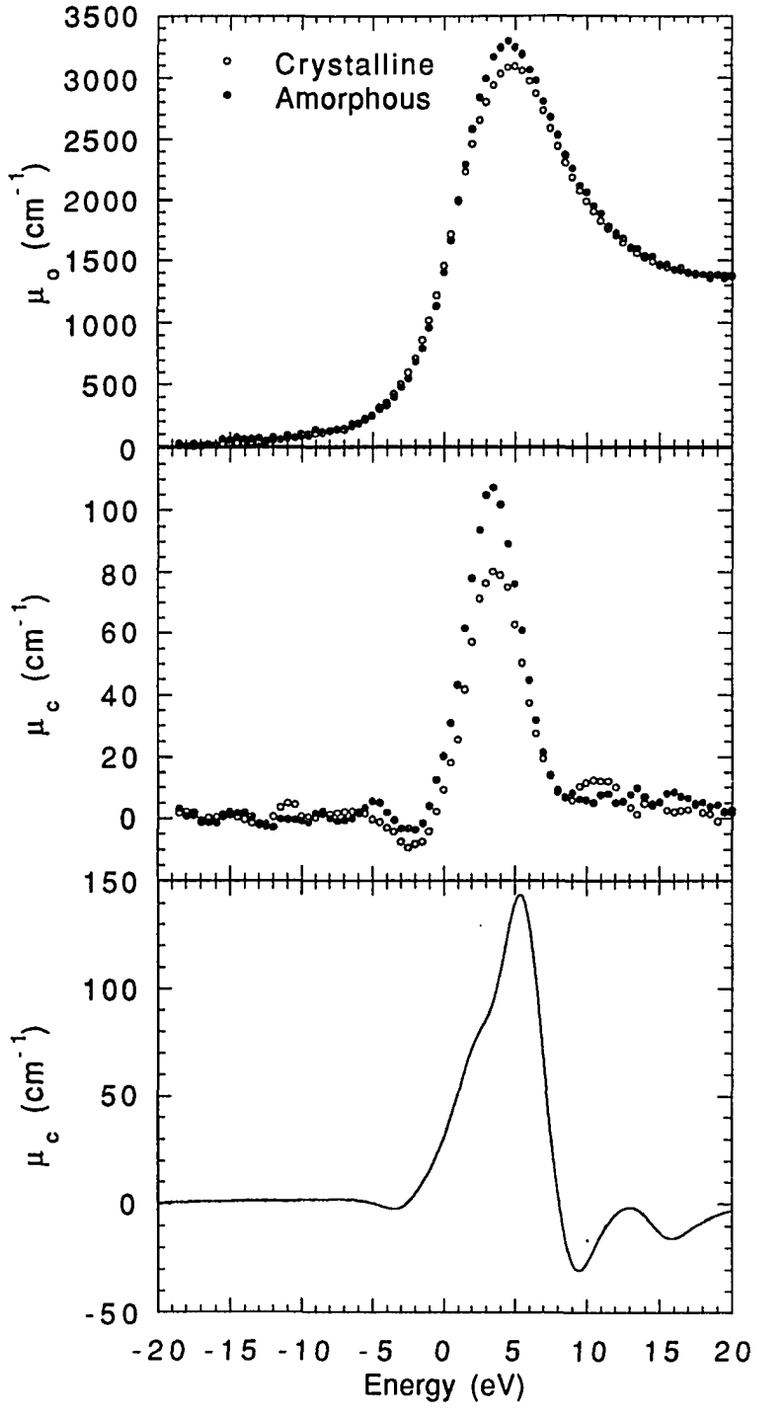

Figure 2 Dichroism at the Gd L_3 edge. Top: Absorption of crystalline and amorphous samples. Middle: Dichroism signal μ_c of crystalline and amorphous samples. Bottom: Theoretical curve for crystalline $GdFe_2$.

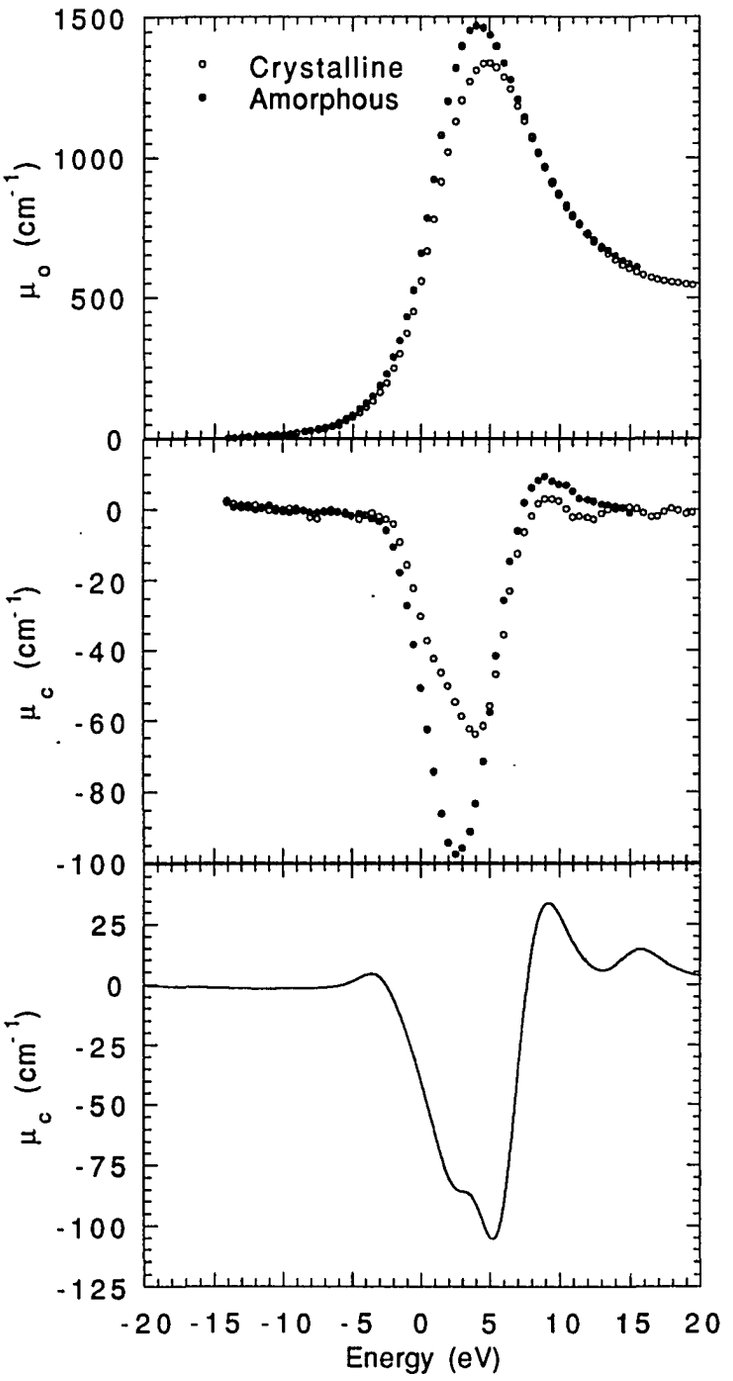

Figure 3 Dichroism at the Gd L_2 edge. Top: Absorption of crystalline and amorphous samples. Middle: Dichroism signal μ_c of crystalline and amorphous samples. Bottom: Theoretical curve for crystalline $GdFe_2$.

Table 1 Integrated intensities A and widths W for each of the edges. Values for the Fe K edge are for features B and C of figure 1. The orbital moments are calculated using the sum rule derived in reference 19.

	A(K)	W(K) (eV)	$A(L_2)$	$W(L_2)$ (eV)	$A(L_3)$	$W(L_3)$ (eV)	$\langle L_z \rangle$ (μ_b)
Amorphous	-8.0,6.8	2.5,2.0	-465	5.0	508	4.5	.005±.003
Crystalline	-7.0,5.7	2.0,2.0	-303	6.0	454	5.0	.018±.005
Theory	-34.6,24.8	2.0,2.0	-440	4.5	570	4.0	.014

The theoretical dichroic spectra at the L_2 and L_3 edges reproduce the general features observed in the experimental spectra. The theoretical curves, however, demonstrate more pronounced structure than experiment. We believe that this is due to the neglect of core-hole effects. The inclusion of core hole effects would draw in, and narrow, the 5d band compressing the signal near the Fermi energy, as observed in experiment. As stated previously, the sum rules are not affected by the core hole, since they involve an integration over all states. The value of the 5d orbital moment observed by experiment .018±.005μ_b for crystalline $GdFe_2$ is within error of the value obtained from theory, .014μ_b. The experimental values, however, neglect the possible contributions due to the presence of quadrupole transitions to the 4f states in the CMXD signal, since the total spectra were integrated. Applying the sum rules to the theoretical spectra with the quadrupole contributions included yields a value of .017μ_b. Thus it is expected that the experimental value obtained should be slightly higher than the

true 5d orbital moment.

We have demonstrated that the differences in the spin dependent band structure between amorphous and crystalline materials are easily observable by CMXD. Further, it has been shown that the differences can be quantified using the recently derived sum rules to obtain the size of the orbital moments. The degree of spin-orbit coupling present in the sample is consistent with band structure calculations. This information should prove valuable in analyzing the magnetic and magneto-optical properties of amorphous rare earth-transition metal materials. The theoretical calculations are being extended to include estimates of the core hole effects and the changes in electronic structure for the amorphous ground state. Since these calculations are much more involved, they will be reported elsewhere. We expect that, with the advent of third generation synchrotron sources, CMXD should become an increasingly important tool to probe the magnetic properties of different magnetic materials.

ACKNOWLEDEGMENTS

Ames Laboratory is operated for the United States Department of Energy by Iowa State University under contract No. W-7405-ENG-82. Work at CHESS was supported by the National Science Foundation under grant No. DMR-87-19764.

REFERENCES

* Present address, Advanced Photon Source, Bldg. 316, Argonne Natl. Lab., Argonne, IL 60439.

1 G. Schütz, M. Knülle, R. Wienke, W. Wilhelm, W. Wagner, P. Kienle, and R. Frahm, *Z. Phys. B* **73**, 67 (1988).

2 P. Fisher, G. Schütz, and G. Wiesinger, *Sol. State Comm.* **76**, 777 (1990).

3 F. Baudelet, C. Brouder, E. Dartyge, A. Fontaine, J.P. Kappler, and G. Krill, *Europhys. Lett.* **13**, 787 (1990).

4 P. Rudolf, F. Sette, L.H. Tjeng, G. Miegs, and C.T. Chen, *J. Mag. Magn. Mat.* **109**, 109 (1992).

5 J.Ph. Schille, Ph. Sainctavit, Ch. Cartier, D. Lefebvre, C. Brouder, J.P. Kappler, and G. Krill, *Sol. State Comm.* **85**, 787 (1993).

6 S. Rüegg, G. Schütz, P. Fischer, R. Wienke, W.B. Zeper, and H. Ebert, *J. Appl. Phys.* **69**, 5655 (1991).

7 Y. Wu, J. Stöhr, B.D. Hermsmeir, M.G. Samant, and D. Weller, *Phys. Rev. Lett.* **69**, 2307 (1992).

8 P. Carra, B.T. Thole, M. Altarelli, and X. Wang, *Phys. Rev. Lett.* **70**, 2307 (1993).

9 P. Fischer, G. Schütz, S. Scherle, M. Knülle, S. Stähler, and G. Wiesinger, *Sol. State Comm.* **82**, 857(1992).

10 J.J. Rhyne in Handbook on the Physics and Chemistry of Rare Earths Vol. 2, Ch. 16, eds. K.A. Gschneidner Jr. and L. Eyrling (North-Holland, Amsterdam, 1979) .

11 K.H.J. Buschow in Handbook on the Physics and Chemistry of Rare Earths

Vol. 7, Ch. 52, eds. K.A. Gschneidner Jr. and L. Eyrling (North-Holland, Amsterdam, 1983).

12 H. Ebert, P. Strange, and B.L. Gyorfly, *J. Appl. Phys.* **63**, 3055 (1988).

13 R. Wienke, G. Schütz, and H. Ebert, *J. Appl. Phys.* **69**, 6147 (1991).

14 P. Carra, B.N. Harmon, B.T. Thole, M. Altarelli, and G.A. Sawatzky, *Phys. Rev. Lett.* **66**, 2495 (1991).

15 J.C. Lang, S.W. Kycia, X. Wang, B.N. Harmon, A.I. Goldman, D.J. Branagan, R.W. McCallum and K.D. Finkelstein, *Phys. Rev. B* **46**, 5298 (1992).

16 K. Shimomi, H. Maruyama, K. Kobayashi, A. Koizumi, H. Yamazaki, and T. Iwazumi, *Jpn. J. Appl. Phys.* **32-2**, 314 (1992).

17 X. Wang, T.C. Lueng, B.N. Harmon, and P. Carra, *Phys. Rev. B* **47**, 9087 (1993).

18 See for example, B.N. Harmon and A.J. Freeman, *Phys. Rev. B* **10**, 1979 (1974) and references therein.

19 B.T. Thole, P. Carra, F. Sette, and G. van der Laan, *Phys. Rev. Lett.* **68**, 1943 (1992)..

20 M. Blume and D. Gibbs, *Phys. Rev. B* **37**, 1779 (1988).

21 Doon Gibbs, D.R. Harshman, E.D. Isaacs, D.B. McWhan, D. Mills, and C. Vettier, *Phys. Rev. Lett.* **61**, 1241 (1988).

22 C. Vittoria, P. Lubitz, and V. Ritz, *J. Appl. Phys.* **49**, 4908 (1978).

23 Values for the absorption were obtained using the Icsc program developed at the University of Washington.

24 Skriver, H.L., The LMTO method: muffin-tin orbitals and electronic structure (Springer-Verlag, New York, 1984).

25 G. Materlik, J.E. Müller, and J.W. Wilkins *Phys. Rev. Lett.* **50**, 267 (1983).

26 S. Stähler, G. Schütz, and H. Ebert, *Phys. Rev. B* **47**, 818 (1993).

27 G.S. Cargill III, *Solid State Phys.* **30**, 227 (1975).

28 M.S.S. Brooks, L. Nordström, and B. Johansson, *Physica B* **172**, 95 (1991).

GENERAL CONCLUSIONS

The angular dependence of all the features in the dichroic spectra at the L_2 and L_3 edges of grain oriented $REFe_2$ and the L_3 edge of nanocrystalline $Er_2Fe_{14}B$ was found to be consistent with dipolar transitions. Angular averaging calculations indicate that although the size of the angular dependence for pure quadrupole transitions should be diminished it should still be observable for the M' values of the grain aligned samples employed. One possible explanation for the lack of a clear quadrupolar signal is the presence of 4f-5d hybridization which may mask the effect in the dichroism spectra, but not in XRES measurements. While XRES measurements performed on Ho metal[4] clearly show a quadrupole-like feature below the absorption edge,[36] these measurements do not rule out the presence of significant dipole transitions at this same energy. Furthermore, the calculations of the angular dependence were made using an isolated ion approximation, which completely neglected the possible hybridization of the 4f-shell with the conduction electron states both in the ground state and the excited states. When hybridization effects are taken into account, the feature below the edge will have some mixed character due to the transitions from 2p core state states with a mixture of d and f. The mixing of these dipolar transitions below edge will reduce the relative weight of the quadrupolar transitions and make the experimental identification of the angular dependence of the feature more difficult. Although this hybridization must be very small because the 4f states remain highly localized, their effects may be enhanced by the dipolar matrix element which is two orders of magnitudes larger than the quadrupolar matrix element. Thus, it is believed that the basic physics involved in the feature below the edge involves transitions to the localized 4f states, although

some detailed modifications are required to resolve the discrepancies between theory and experiment. Future experiments on this question should be carried out at low temperatures and high fields in order to insure that a maximum orientation of the moments (i.e. M'≈1) is achieved, since even with hybridization the feature below the edge should still exhibit some quadrupolar angular dependence in dichroism measurements.

This study has also shown that the differences in the spin dependent band structure between amorphous and crystalline materials are easily observable by CMXD. Further, it has been shown that the differences can be quantified using the recently derived sum rules to obtain the size of the orbital moment. The substantial quenching of the orbital moment of the amorphous sample, .005±.003μ_b, compared with the crystalline, .018±.005μ_b, is believed to be due to a combination of the smaller net spin moment and the greater crystal field asymmetry found in the amorphous sample. This information should prove valuable in analyzing the magnetic and magneto-optical properties of amorphous rare earth-transition metal materials.

Circular magnetic x-ray dichroism is still a young technique with a great deal of experimental and theoretical work yet to be performed. The unique information provided by CMXD, not available by any other method, should prove valuable in understanding some of the fundamental problems of magnetism. With the advent of third generation synchrotron sources, CMXD should become an increasingly important tool to probe the magnetic properties of different magnetic materials.

LITERATURE CITED

1 F. de Bergevin and M. Brunel, *Phys. Lett.* **39A**, 141 (1972).

2 D. Gibbs, D.E. Moncton, K.L. D'Amico, J. Bohr and B.H. Grier, *Phys. Rev. Lett.* **55**, 234 (1985).

3 M. Blume and D. Gibbs, *Phys. Rev. B* **37**, 1779 (1988).

4 Doon Gibbs, D.R. Harshman, E.D. Isaacs, D.B. McWhan, D. Mills, and C. Vettier, *Phys. Rev. Lett.* **61**, 1241 (1988).

5 D.B. McWhan, C. Vettier, E.D. Isaacs, G.E. Ice, D.P. Siddons, J.B. Hastings, C. Peters, and O Vogt *Phys. Rev. B* **42**, 6007 (1990).

6 G. van Der Laan, B.T. Thole, G.A. Sawatzky, J.B. Geodkoop, J.C. Fluggle, J.M. Esteva, R. Karnatak, J.P. Remeika and H.A. Dabkowska, *Phys. Rev. B* **34**, 6529 (1986).

7 G. Schütz, W. Wagner, W. Wilhelm, P. Kienle, R. Zeller, R. Frahm, and G. Materlik, *Phys. Rev. Lett.* **58**, 737 (1987).

8 G. Schütz, M. Knülle, R. Wienke, W. Wilhelm, W. Wagner, P. Kienle, and R. Frahm, *Z. Phys. B* **73**, 67 (1988).

9 C.T. Chen, F. Sette, Y. Ma, and S. Modesti, *Phys. Rev. B* **42**, 7262 (1990).

10 P. Rudolf, F. Sette, L.H. Tjeng, G. Miegs, and C.T. Chen, *J. Mag. Magn. Mat.* **109**, 109 (1992).

11 P. Fischer, G. Schütz and G. Wiesinger, *Sol. Stat. Comm.* **76**, 777 (1990).

12 P. Fischer, G. Schütz, S. Scherle, M. Knülle, S. Stähler, and G. Wiesinger, *Sol. State Comm.* **82**, 857 (1992).

13 S. Stähler, G. Schütz, and H. Ebert, *Phys. Rev. B* **47**, 818 (1993).

14 F. Baudelet, C. Brouder, E. Dartyge, A. Fontaine, J.P. Kappler, and G. Krill, *Europhys. Lett.* **13**, 787 (1990).

15 J.Ph. Schille, Ph. Sainctavit, Ch. Cartier, D. Lefebvre, C. Brouder, J.P. Kappler, and G. Krill, *Sol. State Comm.* **85**, 787 (1993).

16 J.Ph. Schille, F. Bertran, M. Finazzi, C. Brouder, J.P. Kappler, and G. Krill, preprint submitted to *Phys. Rev. Lett.*.

17 K. Shimomi, H. Maruyama, K. Kobayashi, A. Koizumi, H. Yamazaki, and T. Iwazumi, *Jpn. J. Appl. Phys.* **32-2**, 314 (1992).

18 K. Kobayashi, H. Maruyama, H. Maeda and H. Yamazaki, *Jpn. J. Appl. Phys.* **32-2**, 311 (1992).

19 S. Rüegg, G. Schütz, P. Fischer, R. Wienke, W.B. Zeper, and H. Ebert, *J. Appl. Phys.* **69**, 5655 (1991).

20 Y. Wu, J. Stöhr, B.D. Hermsmeir, M.G. Samant, and D. Weller, *Phys. Rev. Lett.* **69**, 2307 (1992).

21 F. Baudelet, E. Dartyge, A. Fontaine, C. Brouder, G. Krill, J.P. Kappler, and M. Piecuch, *Phys. Rev. B* **43**, 5857 (1991).

22 P. Carra, B.T. Thole, M. Altarelli, and X. Wang, *Phys. Rev. Lett.* **70**, 2307 (1993).

23 H. Ebert, P. Strange, and B.L. Gyorfly, *J. Appl. Phys.* **63**, 3055 (1988).

24 R. Wienke, G. Schütz, and H. Ebert, *J. Appl. Phys.* **69**, 6147 (1991).

25 J. Goedkoop, Ph. D. Thesis, University of Nijmegen, (1989) and references therein.

26 P. Carra and M. Altarelli, *Phys. Rev. Lett.* **64**, 1286 (1990).

27 P. Carra, B.N. Harmon, B.T. Thole, M. Altarelli, and G.A. Sawatzky, *Phys. Rev. Lett.* **66**, 2495 (1991).

28 X. Wang, T.C. Lueng, B.N. Harmon, and P. Carra, *Phys. Rev. B* **47**, 9087 (1993).

29 B.T. Thole, P. Carra, F. Sette, and G. van der Laan, *Phys. Rev. Lett.* **68**, 1943 (1992).

30 J.Ph. Schille, F. Bertran, M. Finazzi, C. Brouder, J.P. Kappler, and G. Krill, preprint.

31 J.J. Rhyne in Handbook on the Physics and Chemistry of Rare Earths Vol. 2, Ch. 16 eds. K.A. Gschneidner Jr. and L. Eyrling (North-Holland, Amsterdam, 1979).

32 K.H.J. Buschow in Handbook on the Physics and Chemistry of Rare Earths Vol. 7, Ch. 52 eds. K.A. Gschneidner Jr. and L. Eyrling (North-Holland, Amsterdam, 1983).

33 D.P. Siddons, M. Hart, Y. Amemiya, and J.B. Hastings, *Phys. Rev. Lett.* **64**, 1967 (1990).

34 Qun Shen and K.D. Finkelstein, *Phys. Rev. B* **45**, 5075 (1992).

35 E.E. Alp, M. Ramanathan, S. Salem-Sugui, Jr., F. Oliver, V. Stojanoff, and D.P. Siddons, *Rev. Sci. Instrum.* **63**, 1221 (1992).

36 J.P. Hannon, G.T. Trammel, M. Blume, and D. Gibbs, *Phys. Rev. Lett.* **61**, 1245 (1988).

37 C. Brouder, *J. Phys. Cond. Matt.* **2**, 701 (1990).

38 Jackson, J.D., Classical Electrodynamics, Ch. 14, (John Wiley & Sons, New York, 1975).

39 S. Krinsky, M.L. Perlman, and R.E. Watson in Handbook on Sychrotron Radiation, Vol. 1 Ch. 2, (North-Holland, Amsterdam, 1983).

40 Q. Shen and K.D. Finkelstein, *Phys. Rev. Lett.* **65**, 3337 (1990).

41 B. Batterman, *Phys. Rev. B* **45**, 12677 (1992).

42 M. Blume and D. Gibbs, *Phys. Rev. B* **37**, 1779 (1988).

APPENDIX A. ORIGIN OF DICHROIC SIGNAL

The x-ray absorption cross section due to dipole transitions may be written as,[37]

$$\sigma(\varepsilon^{\alpha},\omega)=4\pi^{2}\hbar\alpha\sum_{f,m_j,\alpha}\left|\left\langle f\left|\varepsilon^{\alpha}\bullet r\right|jm_j\right\rangle\right|^{2}\delta(E_f-E_i-\hbar\omega). \tag{A.1}$$

In the above expression the initial core states are strongly spin-orbit coupled, thus can be expressed in terms of $|jm_j\rangle$ states. As an example, consider the above expression for an L_2 edge with initial $2p_{1/2}$ core state. In the rare earths the final states at these edges are primarily the 5d character, since the transition to the 6s states largely suppressed due to the negligible overlap with the initial state. Neglecting any spin-orbit coupling, the 5d band states can be written as the product of a spatial and spin wave functions,

$$\langle f|\ =\ \varphi_{lm}(r)|s\rangle. \tag{A.2}$$

The electric dipole interaction for left- (right-) circular polarization can be written as,

$$\varepsilon^{\pm}\cdot\mathbf{r}=\pm\left[\frac{4\pi}{3}\right]^{\frac{1}{2}}\mathbf{r}\,Y_{1\pm1}. \tag{A.3}$$

The initial $\left|jm_j\right\rangle$ states ($m_j=\pm1/2$ for and L_2 edge) can be expanded in terms of $|lm_l\rangle$ wavefunctions by using Clebsch-Gordan coefficients,

$$\left|\frac{1}{2}-\frac{1}{2}\right\rangle = \phi_{11/2}(r)\left[\sqrt{\frac{1}{3}}Y_{10}\left|\downarrow\right\rangle - \sqrt{\frac{2}{3}}Y_{1-1}\left|\uparrow\right\rangle\right] \tag{A.4}$$

$$\left|\frac{1}{2}\frac{1}{2}\right\rangle = \phi_{11/2}(r)\left[-\sqrt{\frac{1}{3}}Y_{10}\left|\uparrow\right\rangle + \sqrt{\frac{2}{3}}Y_{11}\left|\downarrow\right\rangle\right]. \tag{A.5}$$

If we assume that the spin functions are orthogonal and the radial parts of the wave functions are independent of spin, we can define quantities $\rho^{\uparrow}$ and $\rho^{\downarrow}$ which incorporate all the constants and the radial matrix elements. Here $\rho^{\uparrow}$ ($\rho^{\downarrow}$) represents a transition to a spin up (down) state, which naively can be considered proportional to the spin up (down) spin density of unoccupied states. This is not strictly valid for the $L_{2,3}$ edges of rare earths, however, as pointed out in the discussion of paper III. For left circularly polarized light equation 1 reduces to,

$$\sigma^{+}_{L_2} \sim \frac{1}{3}\left|\langle 21|1\,1|10\rangle\right|^2\rho^{\downarrow} + \frac{2}{3}\left|\langle 20|1\,1|1-1\rangle\right|^2\rho^{\uparrow} + \frac{1}{3}\left|\langle 21|1\,1|10\rangle\right|^2\rho^{\uparrow} + \frac{2}{3}\left|\langle 22|1\,1|1\,1\rangle\right|^2\rho^{\downarrow}. \tag{A.6}$$

Here all the null matrix elements of terms with opposite spin to the factors in equations 4 and 5 above have been omitted and the selection rule $m_f = m_i + 1$ for the integration of three spherical harmonics has been used. Performing the integrations and normalizing this reduces to,

$$\sigma^{+}_{L_2} \sim \frac{3}{5}\rho^{\downarrow} + \frac{12}{5}\rho^{\uparrow} + \frac{3}{5}\rho^{\uparrow} + \frac{2}{5}\rho^{\downarrow} = \rho^{\uparrow} + 3\rho^{\downarrow}. \tag{A.7}$$

Thus, assuming that the radial parts of the matrix elements are spin independent, left circularly polarized light will be three times more likely to make a transition to a

spin down state than a spin up state. Repeating the above steps for right handed circular polarization, just the opposite is obtained,

$$\sigma_{L_2}^{-} \sim 3\rho^{\uparrow} + \rho^{\downarrow}. \tag{A.8}$$

Therefore, right circularly polarized light will make preferential absorption to spin up states. The same procedure can be repeated for the L_3 edge with an initial $2p_{3/2}$ state to obtain the following results for left and right circular polarization,

$$\sigma_{L_3}^{+} \sim 5\rho^{\uparrow} + 3\rho^{\downarrow}, \qquad \sigma_{L_3}^{-} \sim 3\rho^{\uparrow} + 5\rho^{\downarrow}. \tag{A.9}$$

Here the assumption has been made that the $2p_{1/2}$ and $2p_{3/2}$ radial matrix elements are essentially equal,

$$\rho_{1/2}^{\uparrow(\downarrow)} = \rho_{3/2}^{\uparrow(\downarrow)} = \rho^{\uparrow(\downarrow)}. \tag{A.10}$$

Using equations A.7, A.8, and A.9 the following expressions for the normal and dichroic absorption at these $L_{2,3}$ edges can be written,

$$\mu_c(L_2) \sim \sigma^+ - \sigma^- \sim -2\left(\rho^{\uparrow} - \rho^{\downarrow}\right), \qquad \mu_c(L_3) \sim \sigma^+ - \sigma^- \sim 2\left(\rho^{\uparrow} - \rho^{\downarrow}\right),$$

$$\mu_o(L_2) \sim \sigma^+ + \sigma^- \sim 4\left(\rho^{\uparrow} + \rho^{\downarrow}\right), \qquad \mu_o(L_3) \sim \sigma^+ + \sigma^- \sim 8\left(\rho^{\uparrow} + \rho^{\downarrow}\right). \tag{A.11}$$

The dipole allowed transitions at the L_2 and L_3 edges for both incident polarizations are summarized in Figure 1. From the equations A.11 it can be seen

that the normal absorption at the L_3 edge should be twice as large as the absorption at the L_2 edge and the dichroic signals at the two edges should be in a 1:-1 ratio. The observed CMXD signal at the $L_{2,3}$ edges is approximately in this ratio but there are substantial deviations. The neglect of final state spin-orbit coupling in this simple model is responsible for observed deviations from the 1:-1 ratio of the dichroic signal. The spin-orbit interaction would break the degeneracy of the m_l states in Figure 1. This results in an enhancement of the CMXD signal at the L_3 edge at the expense of the L_2 edge signal by an amount dependent on the degree of spin-orbit coupling in the final states. Quantitatively this has been expressed in terms of the sum rule for the orbital moment discussed in the introduction. The same μ_o 2:1 and μ_c 1:-1 ratios are obtained if this analysis is repeated for $M_{4,5}$ edges.

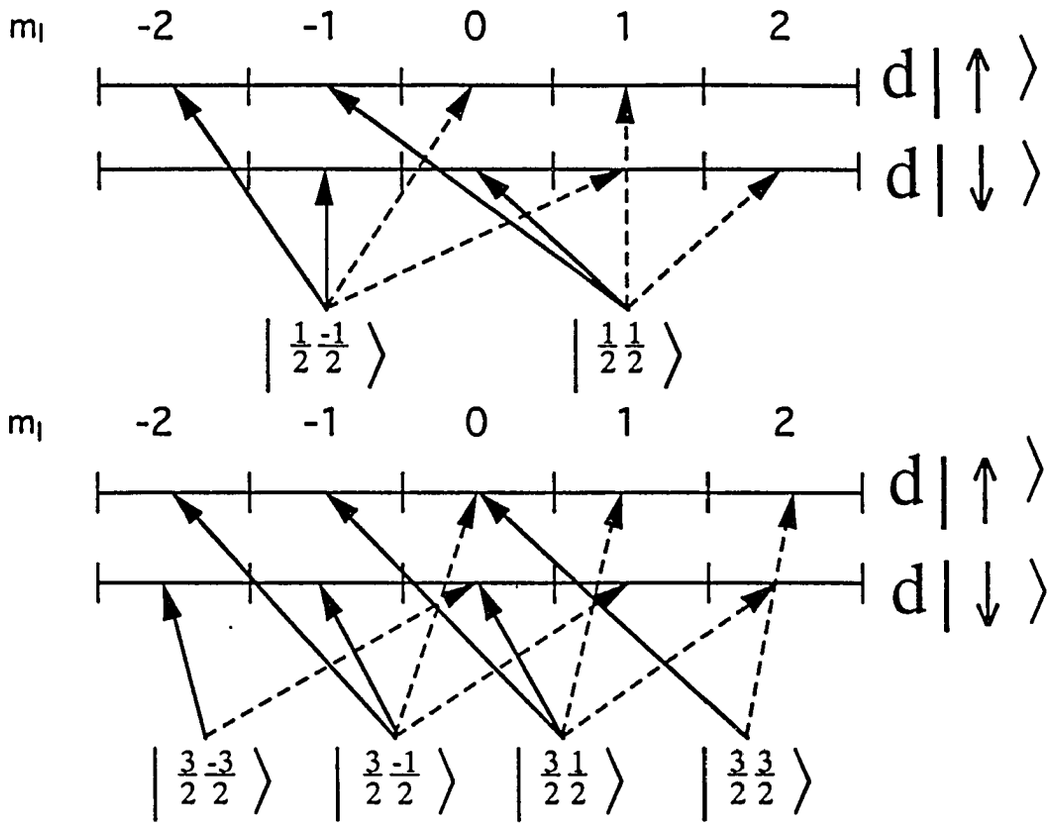

Figure A.1 Dipole allowed transitions at the L_2 (top) and L_3 (bottom) edges. The dashed lines are for left circularly polarized light and the solid lines for right circularly polarized light.

APPENDIX B. POLARIZATION OF SYNCHROTRON RADIATION

Synchrotron radiation is the electromagnetic radiation emitted by relativistic electrons or positrons which are accelerated into curved trajectories by a magnetic field. The spectral distribution and polarization properties of synchrotron light make it by far the best source of hard x-ray radiation. These properties are reviewed in numerous texts and articles;[38,39] only a brief summary of the important properties pertaining to dichroism measurements are presented here. The relativistic particles traversing a circular path emit a cone of radiation tangential to their path centered on the orbital plane. The observation angle with respect to the orbital plane is defined as ψ. The intensity of the radiation emitted as a function of ψ and wavelength λ is given by,[39]

$$I(\lambda,\Psi) = \frac{27}{32\Pi^3}\frac{e^2c}{R}\left(\frac{\lambda}{\lambda_c}\right)^4 \gamma^8 \left(1+(\gamma\psi)^2\right)^2 \left[K_{2/3}^2(\xi) + \frac{(\gamma\psi)^2}{1+(\gamma\psi)^2} K_{1/3}^2(\xi)\right], \qquad \text{(B.1)}$$

where λ_c is the cut off wavelength defined by,

$$\lambda_c = \frac{4}{3}\pi R \gamma^{-3}, \quad \text{and} \quad \xi \equiv \frac{\lambda_c}{2\lambda}\left[1+(\gamma\psi)^2\right]^{3/2}. \qquad \text{(B.2)}$$

In the above equations $\gamma = E/m_0c^2$, R is the bending radius of the orbit, and $K_{2/3}(\xi)$ and $K_{1/3}(\xi)$ are the modified Bessel functions. The first term in the bracket above arises from the solution with the electric field vector in the orbital plane (σ polarization) and the second from the solution with the electric field perpendicular to the orbital plane (π polarization). Notice that at ψ=0 the second term disappears

and the radiation emitted is completely polarized in the orbital plane. The finite extent of the source, however, usually prevents the realization of this complete polarization. The relative intensities of the two polarizations as a function of ψ is shown in Figure B.1 for 8keV photons and typical parameters for a bending magnet beamline at CHESS.

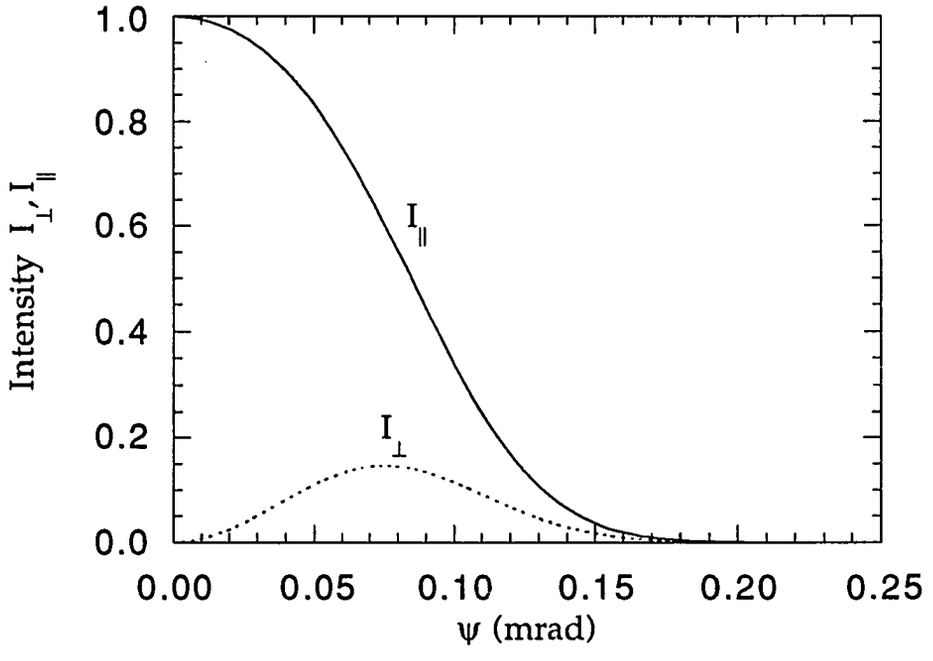

Figure B.1 Normalized intensity of the σ ($I_{||}$) and π ($I_\perp$) polarizations as a function of the off axis angle ψ for 8keV photons at the CHESS D-line.

At $\psi>0$ the two linear polarization components are not an uncorrelated superposition but add up coherently to produce elliptically polarized radiation. We can decompose this into I_R right- and I_L left-handed components to write the degree of circular polarization as,

$$P_c = \frac{I_R - I_L}{I_R + I_L} \qquad (B.3)$$

The degree of circular polarization as a function of ψ is plotted in Figure B.2.

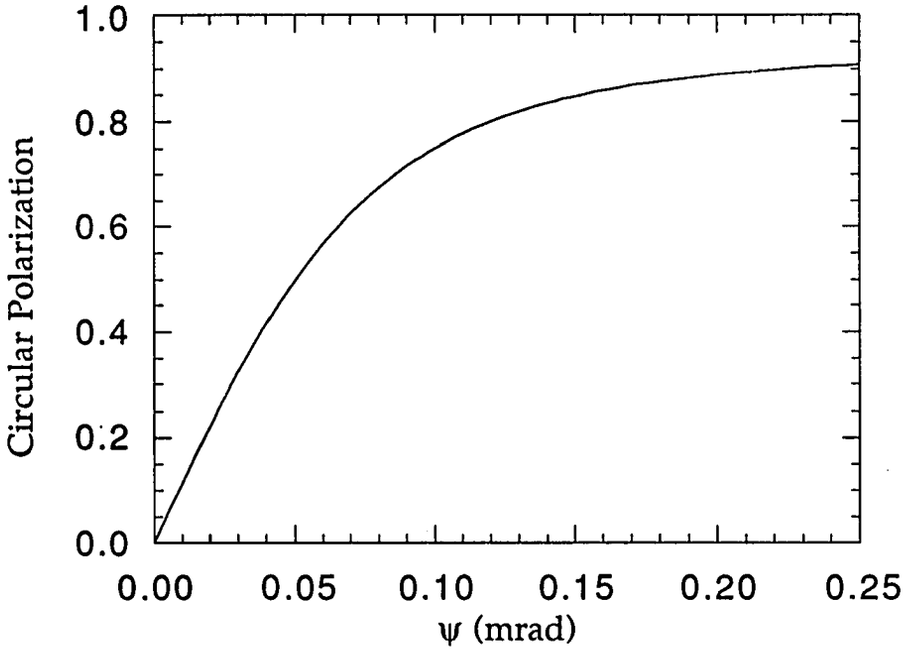

Figure B.2 Degree of circular polarization as a function of off-axis angle for the CHESS D-line.

Thus, by using the synchrotron radiation out of the electron orbital plane we can obtain a high degree of circular polarization. Obtaining circular polarization in this way, however, is done at the expense of beam intensity as seen in Figure B.1. Typically dichroism measurements are performed with the beam intensity about

10% of the ψ=0 value, at which the degree of circular polarization is approximately $P_c \approx .65 \pm .10$. Maintaining of a stable degree of polarization when using off axis x-rays is difficult since a small shift in the electron beam position results in dramatic shifts in intensity and polarization. This is due to the fact that the beam employed is located on the slope of the intensity (see Figure B.1) and polarization (see Figure B.2).

APPENDIX C. DETECTION OF DEGREE OF CIRCULAR POLARIZATION

An multiple beam diffraction (MBD) process occurs when two or more atomic planes satisfy Braggs's law simultaneously inside a crystal. A convenient way to achieve this is to rotate a diffraction crystal around the scattering vector **H**, keeping that Bragg reflection excited. When the crystal is oriented such that another reciprocal lattice point **L** is on the Ewald sphere, a multiple-beam diffraction will occur, which can give rise to a secondary peak in the intensity of the **H** reflection. The reflection **H** is called the main reflection and the reflection **L** is called the detoured reflection. A third reflection **H - L** , the coupling reflection, is required to bring the detoured reflection back into the direction of the main reflection. This is illustrated in Figure C.1.

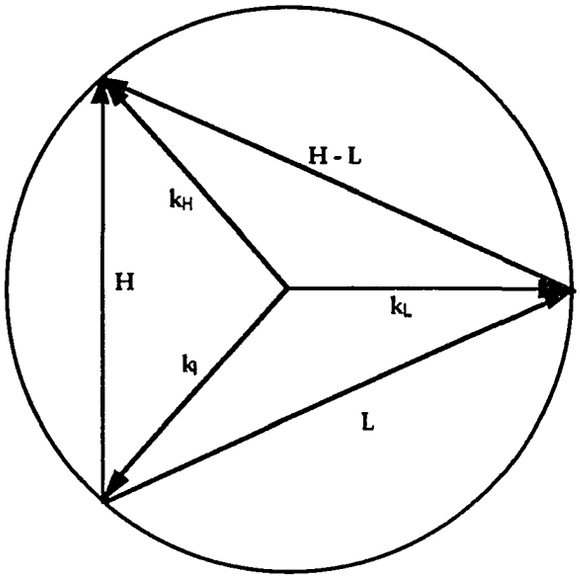

Figure C.1 Ewald sphere showing the showing the main reflection **H**, the detoured reflection **L**, and the coupling reflection **H-L**.

The detour-diffracted (through **L** and **H - L**) and the direct-diffracted beam can interfere with each other and produce an intensity enhancement or reduction pattern in the neighborhood of the multibeam excitation. In general, the two diffracted beams have different phase shifts according to the structure factors of the reflections involved, F_H, F_L, and F_{H-L}, with phases α_H, α_L, α_{H-L}.[40] The interference between the two waves depends on the relative phase shift $\delta_{HL} = \alpha_L + \alpha_{H-L} - \alpha_H$.

When the detour reflection **L** is not in the diffraction plane defined by the main reflection **H**, (out of the paper in Figure C.1), the polarization of the two beams can mix. In other words, each reflection samples a different component of the sigma and pi polarizations. Since there is a phase shift between the σ and π polarizations, the standing waves setup by these reflections can interfere with each other. This phase shift between the two polarizations changes as one passes from one side of the rocking curve of reflection **L** to the other,[41] producing an asymmetric multiple scattering peak with an enhancement on one side and a reduction on the other. This pattern can be fit to obtain the *Poincaré vector of polarization*,[40,42] $\mathbf{P}=(P_1, P_2, P_3)$ where P_1 and P_2 fully define the linear polarization of the beam and P_3 gives the degree of circular polarization.